

# Effects of Shower Partons on Soft and Semihard hadrons Produced in Pb-Pb Collisions at 2.76 TeV

Lilin Zhu<sup>1</sup> and Rudolph C. Hwa<sup>2</sup>

<sup>1</sup>*Department of Physics, Sichuan University, Chengdu 610064, P. R. China*

<sup>2</sup>*Institute of Theoretical Science and Department of Physics*

*University of Oregon, Eugene, OR 97403-5203, USA*

## Abstract

The production of all identified hadrons at the CERN Large Hadron Collider (LHC) is studied with emphasis on the  $p_T$  distributions up to 20 GeV/c in central collisions. In the framework of the recombination model we find that the shower partons (due to the fragmentation of semihard partons) play an important role in the formation of hadrons in the low- and intermediate- $p_T$  regions. Parameters that control the energy loss of minijets are determined by fitting the upper half of the  $p_T$  range of the pion distribution. The resultant soft shower partons are then found to dominate over the thermal partons in the non-strange sector, but not in the strange sector. Since the data on the  $p_T$  spectra of all observed hadrons are well reproduced, there is no way out of the implication that any alternative dynamical model on particle production would be incomplete if it does not consider the effects of minijets even at very low  $p_T$ . Hydrodynamics that relies on rapid equilibration without accounting for the delayed thermalization effects of the hard and semihard partons copiously produced at LHC is an example of such models. The difference between the densities of shower partons produced at LHC and at BNL Relativistic Heavy-Ion Collider (RHIC) is quantified and discussed.

## I. INTRODUCTION

Theoretical investigation of hadron production in heavy-ion collisions at high energies is usually separated into different camps, characterized by the regions of transverse momenta  $p_T$  of the produced hadrons. At low  $p_T$  statistical hadronization and hydrodynamical models are generally used [1–5], whereas at high  $p_T$  jet production and parton fragmentation with suitable consideration of medium effects in perturbative QCD are the central themes [6–10]. The two approaches have been studied essentially independent of each other with credible success in interpreting the data, since their dynamics are decoupled at the energies investigated. The situation may have changed at the CERN Large Hadron Collider (LHC), where Pb-Pb collisions have been carried out at  $\sqrt{s_{NN}} = 2.76$  TeV, resulting in thousands of soft hadrons on the one hand, and multiple hard jets on the other. Minijets that are copiously produced at intermediate  $p_T$  can fragment into soft partons with multiplicities so high that their effects on the hadronization of all partons created in the soft sector cannot be ignored. It is the aim of this paper to investigate what those effects are and to offer an explanation of the observed hadronic spectra of all species and for all  $p_T$  measured up to 20 GeV/c.

Hard parton scattering and hydrodynamical flow are processes that involve very different time scales. It would be hard to incorporate them into a unified formalism that describes all aspects of the system, including thermalization time, initial configuration, fluid nature of the medium, its quenching effect on the hard protons, the creation of shower partons, and the hadronization of all partons at the end of the whole process. Our attempt here is far from being so ambitious. We focus only on the  $p_T$  dependencies of the hadrons produced from 0.5 to 20 GeV in a formalism that can be valid throughout that range, provided that we use some model inputs for the thermal component of the low- $p_T$  behavior to supplement the hard component that can be calculated at high  $p_T$ . We use quark recombination to treat hadronization, applied uniformly at all  $p_T$ . In treating the degradation of momenta of hard and semihard partons we shall adjust some parameters to fit the high- $p_T$  data. Since we aim to confront the  $p_T$  spectra of all observed hadrons,  $\pi$ ,  $K$ ,  $p$ ,  $\Lambda$ ,  $\Xi$ ,  $\phi$  and  $\Omega$ , the system is highly constrained. The primary feature of this study is to quantify the effect of hard and semihard jets on the soft sector. What we find is that the soft partons generated by the hard partons are so much more at LHC, compared to the situation at RHIC, that any

treatment without including that aspect of the problem would be incomplete.

Our investigation of produced hadrons with various contents of strangeness also reveals contrasting features of heavy-ion physics not commonly addressed. Whereas hard scattering of gluons and light quarks can readily occur at high energies, jet fragmentation into multi-strange hadrons like  $\Omega$  and  $\phi$  is rare even at LHC. But the production of  $\Omega$  relative to  $p$  grows exponentially with  $p_T$  even to the highest  $p_T$  measured, the data for which will be exhibited explicitly in the next section. Surely, one cannot expect  $\Omega$  to be easily produced at  $p_T = 7$  GeV/c by jet fragmentation. An explanation of the observed phenomenon must be an integral part of a description of the production mechanism of all hadrons.

To give a description of the experimental motivation for our study, we show in Sec. II several pieces of data presented in novel ways so as to emphasize the problems that have not been commonly discussed. It will become clear that the hadronization problem at LHC is drastically different from that at RHIC. In the framework of the recombination models [11–14] in which the partons just before hadronization are categorized into thermal (T) and shower (S) partons, that difference at LHC can be succinctly stated in the form that S is much greater than T at low  $p_T$  for light quarks, but not strange quarks. Such a statement has no phenomenological consequence unless the hadronization of those quarks is treated by recombination.

We do not consider here other features of heavy-ion collisions besides  $p_T$  distributions, most notably the azimuthal dependence in non-central collision. Conventional description of elliptic flow does not consider the effects of jets. We shall treat that subject separately, after our concern about the shower partons establishes a footing in the general terrain of heavy-ion physics.

To clarify the nature of our approach it is necessary to contrast it from the standard model based on hydrodynamics. If hard and semihard partons produced in high-energy-energy nuclear collisions are important in their effects on soft particles, then one should recognize that their in-medium radiated daughter partons take some time to thermalize, much longer than the rapid equilibration time ( $\tau_0 \sim 0.6$  fm/c) usually assumed in hydro calculations. A hard parton produced near the center of the medium in central collisions would take about 6 fm/c to reach the surface. Thus rapid thermalization is not realistic if minijets are important, as we shall show that they are at LHC. As a consequence, we cannot make use of hydro results in our approach, nor can hydro results be used to censure

our calculations. For example, the thermal parton distribution that we consider is not to be identified with any distribution of the fluid constituents in the hydro medium. Also, in the hydro treatment  $v_2$  is identified with elliptic flow, but it is only a possible, not a necessary, explanation. Other explanations are also possible; see, for example, Refs. [15–17]. In this paper we consider only central collisions and establish the importance of shower partons at low momenta. It is suggested that a reader withhold comparison with hydro treatment until the main points advanced here can be made.

This paper is organized as follows: In Sec. II we show experimental features that motivate this investigation. Section III describes the general formulation of our approach to the problem. Shower parton distributions are discussed in detail in Sec. IV with emphasis on how the degradation of parton momenta is treated. With those partons shown to be dominant, the recombination of shower partons from nearby jets becomes a possibility that is considered in Sec. V. With all the basic inputs on partons at hand we then proceed to the determination of the transverse-momentum distributions of  $\pi, p, K$  and  $\Lambda$  in Sec. VI. Multi-strange hyperons and meson are treated in Sec. VII with detail equations given in the Appendices. Section VIII contains our conclusion.

## II. MOTIVATING EXPERIMENTAL FEATURES

We show first some data from LHC that can be taken to suggest something unusual about the usual observables. Compared to the data at RHIC energies and below, it seems that simple extrapolation to Pb-Pb collisions at 2.76 TeV is likely to miss some new physics.

The charged-particle multiplicity density averaged over  $|\eta| < 0.5$  for 0-5% central collisions is shown in Fig. 1 as a function of collision energy  $\sqrt{s_{NN}}$  [18]. What is notable is that a straight line can be drawn through all the points in the semilog plot from  $\sqrt{s_{NN}} = 2.5$  GeV to 200 GeV, but at 2.76 TeV the LHC data point deviates significantly from the straight-line extrapolation. A power-law fit can be made to connect the RHIC and LHC points for  $\sqrt{s_{NN}} > 10$  GeV, as shown in [19], resulting in the behavior  $\propto s^{0.15}$ , but that would overlook the distinctive feature of the LHC point. The dramatic increase above the logarithmic dependence suggests the onset of new physics.

Another difference between LHC and RHIC is the dependence on  $p_T$ . From the  $p_T$  distributions measured at the two energies, 2.76 and 0.2 TeV, we can calculate their ratio. When

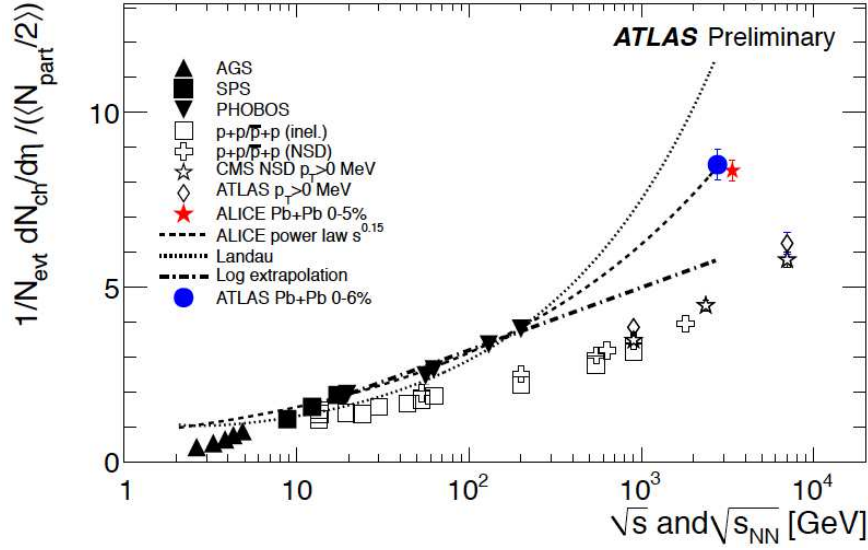


FIG. 1: (Color online) Inclusive charged particle multiplicity per participant pair as a function of collision energy, measured for the 6% most central collisions, compared with the lower energy data. This figure is from Ref. [18].

the data points are not in the same  $p_T$  bin, we make Lagrangian interpolation between adjacent bins in the RHIC data [20, 21] to match the LHC bin [22, 23]. The result for pion is shown by the solid (black) line in Fig. 2. Note the exponential increase by two orders of magnitude as  $p_T$  is increased up to 10 GeV/c. Similar increases are noted for  $p$  and  $\Omega$  up to  $p_T \sim 6$  GeV/c. The ratios are all around 2 for  $p_T < 1$  GeV/c, consistent with what we see in Fig. 1 where the LHC/RHIC ratio of the multiplicity densities at mid-rapidity per participant-pair is  $\approx 8.5/4 \approx 2$ . Of course, most of the particles contributing to that ratio are pions with  $p_T \lesssim 1$  GeV/c. But for  $p_T > 2$  GeV/c, there are abundantly more particles produced at LHC than at RHIC. It is not unexpected that more high- $p_T$  particles are produced at higher collision energy. The question is what effects do the hard scatterings of partons have on the production of intermediate- $p_T$  hadrons at  $2 < p_T < 6$  GeV/c. Furthermore, it is reasonable to ask whether the physics at low  $p_T$  can be treated by hydrodynamics as at RHIC, totally decoupled from the physics at high  $p_T$ . If jets are copiously produced in order to account for a factor of  $10^2$  at  $p_T \sim 10$  GeV/c in Fig. 2, why would their fragmentation products not populate the low- $p_T$  region below 2 GeV/c? Our knowledge on fragmentation functions derived by leptonic collisions tells us that the distribution of hadronic products

increased monotonically with decreasing momentum fraction [24].

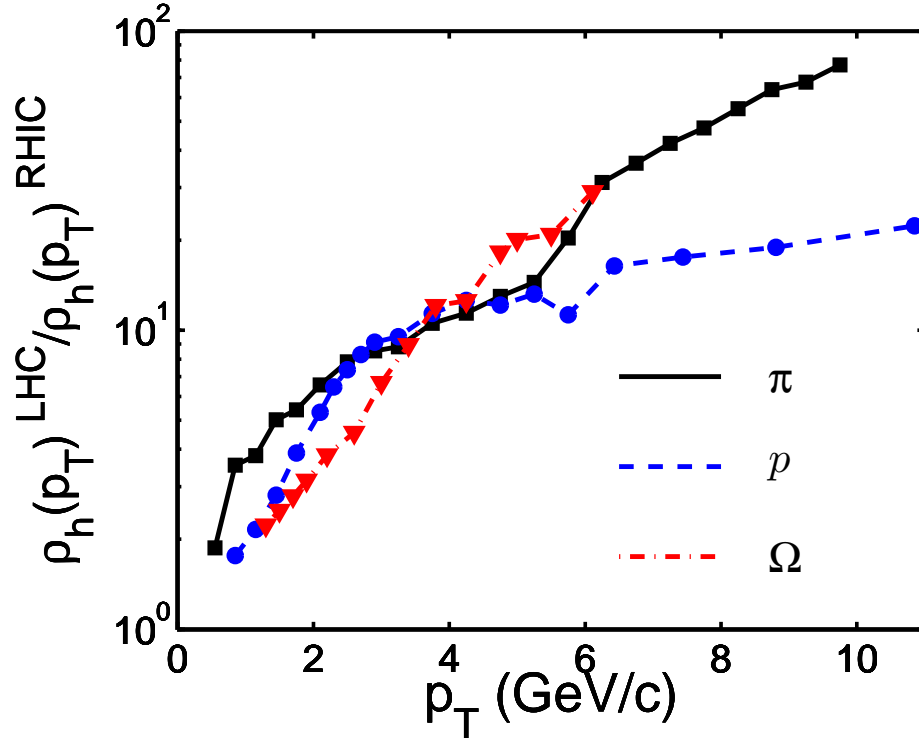


FIG. 2: (Color online) With  $\rho_h(p_T)$  denoting  $dN_h/dp_T d\eta|_{\eta \approx 0}$ , the ratios  $\rho_h^{\text{LHC}}(p_T)/\rho_h^{\text{RHIC}}(p_T)$  vs  $p_T$  are shown for  $h = \pi, p, \Omega$ . The data are from [20–23].

Finally, we show another plot of data from LHC that is thought provoking. From the  $p_T$  distributions of  $p$  and  $\Omega$  measured by ALICE [22, 23], we plot their ratio vs  $p_T$  as shown by the solid (black) line in Fig. 3. The general trend is an exponential rise up to the highest available  $p_T$  with an increase of a factor of 10. The conventional understanding of hadrons produced at  $p_T \sim 7$  GeV/c is by the fragmentation of hard scattered gluons or light-quarks. However,  $s$ -quark jets are highly suppressed; moreover, even if an  $s$  quark is produced at high  $p_T$ , its fragmentation into  $\Omega$  is even more suppressed. To our knowledge it has never been measured, let alone at  $p_T = 7$  GeV/c. Figure 3 shows that the  $\Omega/p$  ratio at RHIC in dashed (red) line also grows exponentially until  $p_T \approx 3$  GeV/c and then decreases slowly. The phenomena at both energies are clearly calling for an explanation.

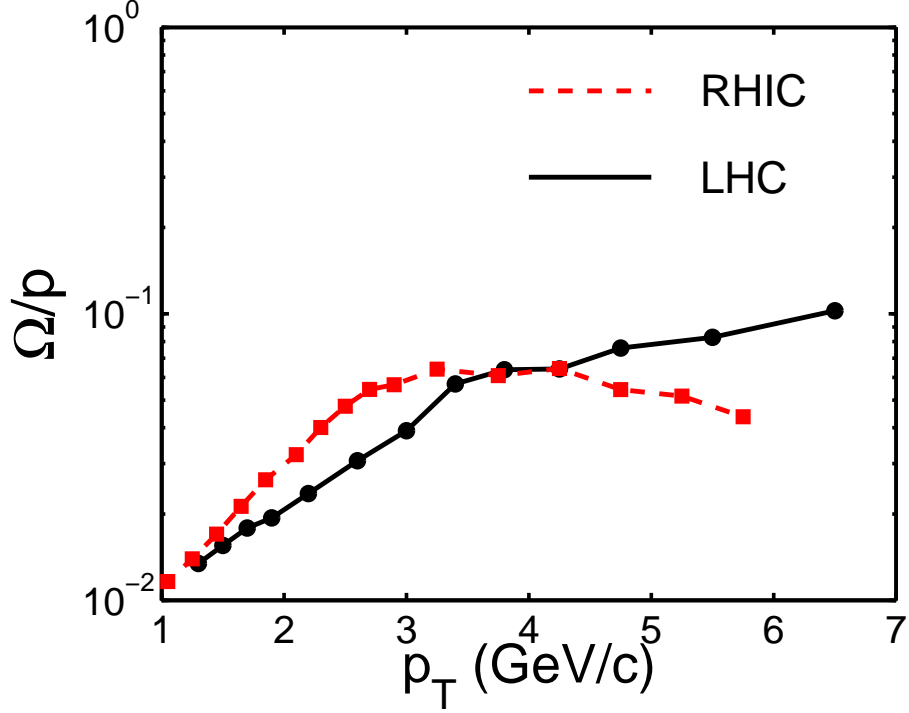


FIG. 3: (Color online) The ratio  $\Omega/p$  vs  $p_T$  for central collision at RHIC and LHC. The data are from [20–23].

### III. FORMULATION OF THE PROBLEM

To calculate the  $p_T$  distribution at mid-rapidity for all hadrons, we use the same formalism as described earlier for Au-Au collisions at 200 GeV [11, 14, 25] and for Pb-Pb collisions at 2.76 TeV [13], i.e., the recombination of thermal and shower partons. We shall use an improved version of the treatment of momentum degradation [26] and adjust the degradation parameters to fit the LHC data over a wider range of  $p_T$ . As a consequence, the study in Ref. [13] for  $p_T < 5$  GeV/c is superseded because the inclusion of harder jets up to 30 GeV/c with less momentum degradation results in a profusion of soft shower partons. Furthermore, we shall include also the production of multi-strange hadrons. The high density of shower partons introduces another complication, which is the recombination of partons from different, but adjacent, jets. Although that component turns out not to be dominant, its effect is not negligible and must be calculated so as to ascertain its magnitude.

The basic framework that describes the recombination of thermal and shower partons at

midrapidity is straightforward [11, 13, 14, 25]

$$p^0 \frac{dN^M}{dp_T} = \int \frac{dp_1}{p_1} \frac{dp_2}{p_2} F_{q_1 \bar{q}_2}(p_1, p_2) R_{q_1 \bar{q}_2}^M(p_1, p_2, p_T) \quad (1)$$

$$p^0 \frac{dN^B}{dp_T} = \int \left[ \prod_{i=1}^3 \frac{dp_i}{p_i} \right] F_{q_1 q_2 q_3}(p_1, p_2, p_3) R_{q_1 q_2 q_3}^B(p_1, p_2, p_3, p_T) \quad (2)$$

The essence is in the details of what the symbols mean. The LHS of Eqs. (1) and (2) are the invariant  $p_T$  distributions of meson and baryon, respectively, averaged over  $\eta$  at midrapidity and over all  $\phi$ . They appear as invariant distributions in the 1D momentum space, but are derived from the invariant distribution in 3D as follows:

$$p^0 \frac{dN}{dp_T} = p^0 p_T \frac{1}{\Delta y} \int_{\Delta y} dy \frac{1}{2\pi} \int_0^{2\pi} d\phi p^0 \frac{d^3 N}{d^3 p} \quad (3)$$

with  $\Delta y$  being a narrow interval at  $y \approx 0$ , say from  $-0.5$  to  $+0.5$ . Thus our formalism here is not framed to address the global properties of the nuclear collisions, such as total charge multiplicity or long-range correlation. The parton momenta  $p_i$  are the transverse momenta (with the subscript  $T$  omitted) of the coalescing quarks.  $R^M$  and  $R^B$  are the recombination functions (RFs) for meson and baryon, respectively. The central issue in the formalism is the determination of the parton distribution  $F_{q_1 \bar{q}_2}$  and  $F_{q_1 q_2 q_3}$  just before hadronization. Because we intend to treat hadron produced in as wide a range in  $p_T$  as experimental data on identified particles are available (for pion up to 20 GeV/c), we must consider partons that are produced in soft, semihard and hard scatterings. We group them into two classes of partons, thermal (T) and shower (S), and use  $\mathcal{T}$  and  $\mathcal{S}$  to denote their invariant distributions in  $p_i$ . Taking into account the recombination of different types of partons, we thus have

$$F_{q_1 \bar{q}_2} = \mathcal{T}\mathcal{T} + \mathcal{T}\mathcal{S} + \mathcal{S}\mathcal{S} \quad (4)$$

$$F_{q_1 q_2 q_3} = \mathcal{T}\mathcal{T}\mathcal{T} + \mathcal{T}\mathcal{T}\mathcal{S} + \mathcal{T}\mathcal{S}\mathcal{S} + \mathcal{S}\mathcal{S}\mathcal{S} \quad (5)$$

We do not commit ourselves to any specific hydrodynamical description of the soft partons, a position that is made more reasonable when, as will be seen below, low- $p_T$  hadrons can be strongly influenced by shower partons at LHC, thus rendering hydro approach to be inadequate even at low  $p_T$ . It dose not mean that we do not recognize the picture that the hot and dense medium created in heavy-ion collision expands. We leave open the issues concerning equilibration time, viscosity, freeze-out dynamics, etc., since undetermined parameters cannot be adjusted to fit the data at low  $p_T$  when the effects of shower partons



cannot be ignored. More specifically, we are concerned with the copious production of hard and semihard jets, whose initiating partons can take up to  $\mathcal{O}(10)$  fm/c to reach the surface, depending on where they are created in the overlapping nuclei and which directions they move in the transverse plane. They can radiate gluons along their in-medium trajectories, and those gluons would take a long time to thermalize with the soft partons in the medium, longer than the short thermalization time  $\tau_0 \sim 0.6$  fm/c assumed in hydrodynamical treatment. The effects of such hard and semihard partons may be ignored in the soft region if they are rarely produced, as at lower collision energies. But at LHC they are important and cannot be neglected. If the basic tenets of hydro are not reliable, the notion of what is thermal must be liberated from the constraints of hydrodynamics. The shower partons generated in the medium interact with the bulk partons, and cannot be distinguished from the latter by the time the density of all soft partons is low enough for hadronization. They are all referred to here as thermal partons in the final stage of the quark matter as they move out of the deconfinement phase. The shower partons that we consider are the fragmentation products of the hard and semihard partons that emerge from the surface after momentum degradation. They are distinguished from the thermal partons that are in their environment. Those are the  $\mathcal{T}$  and  $\mathcal{S}$  in Eqs. (4) and (5).

We use a simple exponential form to represent the thermal parton distribution

$$\mathcal{T}(p_1) = p_1 \frac{dN_q^T}{dp_1} = C p_1 e^{-p_1/T} \quad (6)$$

with the dimensionless prefactor  $C p_1$  necessary to yield pure exponential behavior for the pion distribution  $dN^\pi/p_T dp_T \propto C^2 \exp(-p_T/T)$  arising from TT recombination only, as observed at RHIC [11, 17]. Thus  $C$  has the dimension of inverse momentum. The values of the parameters  $C$  and  $T$  will be discussed below. When shower partons are important at low  $p_T$ , then TS and SS components need to be included. Nevertheless, we retain the form of  $\mathcal{T}(p_1)$  in Eq. (6) for the thermal component.

The shower parton distribution after integration over jet momentum  $q$  and summed over all jets is

$$\mathcal{S}^j(p_2) = \int \frac{dq}{q} \sum_i \hat{F}_i(q) S_i^j(p_2, q), \quad (7)$$

where  $\hat{F}_i(q)$  is the distribution of hard or semihard parton of type  $i$  at the medium surface after momentum degradation while transversing the medium but before fragmentation.  $\hat{F}_i(q)$

was introduced previously for collisions at RHIC for any centrality [17, 26], but will be modified below to suit our description of the physics at LHC.  $S_i^j(z)$  is the unintegrated shower-parton distribution (SPD) in a jet of type  $i$  fragmentation into a parton of type  $j$  with momentum fraction  $z$ . It is determined from the fragmentation function (FF) on the basis that hadrons in a jet are formed by recombination of the shower partons in the jet [27, 28]. In particular, the recombination of a quark  $j$  with an antiquark  $\bar{j}$  in a jet of type  $i$  forms a pion, for which the FF is  $D_i^\pi(z_j + z_{\bar{j}})$ . The numerical form for  $S_i^j(z_j)$  can therefore be calculated from the data on  $D_i^\pi$  and the RF for pion.

The RFs were introduced a long time ago [29, 30] and have been applied successfully to many collision processes [11–13, 17, 31, 32]. Here for brevity we give only the RFs for pion and proton, leaving other hadrons to be specified later as the cases arise,

$$R_{q\bar{q}}^\pi(p_1, p_2, p_T) = \frac{p_1 p_2}{p_T} \delta(p_1 + p_2 - p_T), \quad (8)$$

$$R_{uud}^p(p_1, p_2, p_3, p_T) = g_{st}^p g_p (y_1 y_2)^\alpha y_3^\beta \delta\left(\sum_i y_i - 1\right), \quad y_i = \frac{p_i}{p_T}, \quad (9)$$

where  $g_{st} = 1/6$ ,  $\alpha = 1.75$ ,  $\beta = 1.05$ , and

$$g_p = [B(\alpha + 1, \alpha + \beta + 2) B(\alpha + 1, \beta + 1)]^{-1}, \quad (10)$$

$B(a, b)$  being the Beta function.

As a note of affirmation, we recall that with these RFs used in Eqs. (1) and (2), and considering only the  $\mathcal{TT}$  ( $\mathcal{TTT}$ ) component for pion (proton), we have been able to fit the pion and proton spectra for  $1 < p_T < 2$  GeV/c in Au-Au collisions at 200 GeV [33] with a common value of the inverse slope in Eq. (6) [17]. For  $p_T < 1$  GeV/c there is resonance contribution that Eq. (1) does not account for, while for  $p_T > 2$  GeV/c shower parton contributions invalidate the approximation of  $F_{q\bar{q}}$  and  $F_{uud}$  by  $\mathcal{TT}$  and  $\mathcal{TTT}$ , respectively. In the  $1 < p_T < 2$  GeV/c interval one may find the excellent agreement with data surprising, when only the exponential form of Eq. (6) is used for both pion and proton, since the proton data for  $dN^p/p_T dp_T$  is not exponential. However, it is precisely because of the momentum dependence in  $R^p$  in Eq. (9) and the fact that  $p_0$  in Eq. (2) is the transverse mass  $m_T(p_T)$  at  $y = 0$  that renders  $dN^p/p_T dp_T$  to deviate from pure exponential. The phenomenological success there gives strong support to the recombination model. As we shall see below, the situation of dominance by TT and TTT recombination changes when the collision energy is increased tenfold, whereby TS and TTS can no longer be neglected. Thus the essence of

this work is to calculate the effects of the shower partons at low and intermediate  $p_T$  region in collisions at LHC.

#### IV. SHOWER PARTON DISTRIBUTIONS

Focusing on the shower partons, we see in Eq. (7) that  $\hat{F}_i(q)$  is the distribution to be determined for collisions at LHC, since  $S_i^j(p_2, q)$  is the SPD outside the nucleon medium and is independent of the collision system; it has been determined previously from FFs in vacuum [27]. At any particular impact parameter  $b$ ,  $\hat{F}_i(q, b)$  is the average over azimuthal angle  $\phi$  of  $\bar{F}_i(q, \phi, b)$ , which has three essential parts [26]

$$\bar{F}_i(q, \phi, b) = \int d\xi P_i(\xi, \phi, b) \int dk k f_i(k) G(k, q, \xi), \quad (11)$$

where  $f_i(k)$  is the parton density in the phase space  $kdk$  at the point of creation,  $k$  being the initial momentum of the hard or semihard parton  $i$ , and  $P_i(\xi, \phi, b)$  is the probability for the parton  $i$  to have a dynamical path length  $\xi$  at  $\phi$  and  $b$ . The two parts are connected by  $G(k, q, \xi)$

$$G(k, q, \xi) = q\delta(q - ke^{-\xi}), \quad (12)$$

which is the momentum degradation function, relating the initial parton momentum  $k$  to the final momentum  $q$  at the medium surface by an exponential decay in  $\xi$ , the length that carries all the geometrical and dynamical information of the process through  $P_i(\xi, \phi, b)$ . The details of calculating  $P_i(\xi, \phi, b)$  are given in Ref. [26] and summarized in the Appendices in Ref. [14]. We shall recall the essence below in order to re-parametrize it for suitable use at LHC.

First, we need to state why we describe momentum degradation in the way outlined above without adopting the results obtained by pQCD in the literature. Because we intend to calculate the  $p_T$  distributions of all hadrons from 1 to 20 GeV/c, we need to let  $q$  in Eq. (7) be integrated from low values in order for the shower partons to have their momenta be as low as 0.5 GeV/c. In practice,  $q$  is integrated from 2 to 30 GeV/c. Low-order perturbative QCD is not reliable for virtuality less than 8 GeV/c, so the major portion of the contribution to the shower partons in the soft region cannot make use of the established theory. Furthermore, the usual calculation based on DGLAP evolution equation is on medium modification of

	$g$	$u$	$d$	$\bar{u}$	$\bar{d}$	$s, \bar{s}$
$A [10^4/\text{GeV}^2]$	6.2	1.138	1.266	0.24	0.23	0.093
$B [\text{GeV}]$	0.98	0.687	0.677	0.87	0.88	1.05
$\beta$	6.22	5.67	5.66	5.97	5.99	6.12

TABLE I: Parameters for  $f_i(k)$  in Eq. (13).

the fragmentation function, while we need shower parton distribution for the purpose of recombination. The dependence on the medium is usually described in terms of entropy density and local flow velocity, which are hydrodynamical quantities tuned to fit low- $p_T$  data, which are exactly what we attempt to reproduce in addition to intermediate- $p_T$  data independent of fluid dynamics. For these reasons we use a phenomenological procedure that has been shown to generate the azimuthal and  $p_T$  dependencies of  $R_{AA}(\phi, p_T)$  at RHIC [26] and can readily be extended to higher energy, as we now proceed to do.

The initial momentum distributions have been determined in Ref. [34] for Au-Au collisions at 200 GeV and Pb-Pb collisions at 5.5 TeV. They are parametrized in the form

$$f_i(k) = K \frac{A}{(1 + k/B)^\beta}. \quad (13)$$

We make logarithmic interpolations of the parameters between the two energies for  $\ln A$ ,  $B$  and  $\beta$  and obtain for  $\sqrt{s_{NN}} = 2.76$  TeV the parameters shown in Table I with  $K = 2.5$ .

The connection between geometry and dynamics is imbedded in the probability function  $P_i(\xi, \phi, b)$ . The geometrical path length  $\ell$ , when written more fully, is

$$\ell(x_0, y_0, \phi, b) = \int_0^{t_1(x_1, y_1)} dt D(x(t), y(t)) \quad (14)$$

that is calculable from nucleon geometry. The transverse coordinate  $(x_0, y_0)$  is the initial point of creation of a hard parton, and  $(x_1, y_1)$  is the exit point. The integration is weighted by the local density,  $D(x, y)$ , along the trajectory, which is marked by the variable  $t$  that does not denote time. As the medium expands, the end point  $t_1(x_1, y_1)$  increases, but  $D(x(t), y(t))$  decreases, so  $\ell$  is insensitive to the details of expansion dynamics. The dynamical path length  $\xi$  is proportional to  $\ell$ , but is to be averaged over all initial points  $(x_0, y_0)$ , i.e.,

$$P_i(\xi, \phi, b) = \int dx_0 dy_0 Q(x_0, y_0, b) \delta(\xi - \gamma_i \ell(x_0, y_0, \phi, b)) \quad (15)$$

where  $Q(x_0, y_0, b)$  is the probability that a hard (or semihard) parton is produced at  $(x_0, y_0)$ , calculable from nucleon thickness functions [14, 26]. The only parameter that we cannot

calculate is  $\gamma_i$ , which incorporate the effects of energy loss during the passage of the parton through the non-uniform and expanding medium. The average dynamical path length  $\bar{\xi}_i$ , defined by

$$\bar{\xi}_i(\phi, b) = \int d\xi \xi P(\xi, \phi, b), \quad (16)$$

depends on geometry, and is proportional to  $\gamma_i$ , as can readily be seen upon substituting Eq. (15) into (16). Thus, using Eqs. (11)-(15),  $\hat{F}_i(q, b)$  can be calculated once  $\gamma_i$  are specified.

In treating hadron production at RHIC we have determined  $\gamma_i$  in Ref. [14] and obtained excellent fits of the  $p_T$  distributions of  $\pi, K, p$  for  $p_T < 10$  GeV/c at all centralities [35–40]. We used  $\gamma_g = 0.14$  for gluon and  $\gamma_q = 0.07$  for all light quarks, their ratio being 2 as an approximation of the color factor  $C_A/C_F = 9/4$ . Because  $\bar{\xi}_i(\phi, b) \propto \gamma_i$ , we have  $\bar{\xi}_g(\phi, b)/\bar{\xi}_q(\phi, b) = 2$ , which directly implies that gluons on average lose the same fraction of momentum as quarks do in half the distance of traversal through the nucleon medium. That turned out to be an important factor in enabling us to reproduce both the pion and proton spectra because at intermediate  $p_T$  pions are more affected by semihard gluon minijets, while protons are more so by quark minijets, due to their recombination characteristics [14].

To extend the treatment of momentum degradation to collisions at LHC, we cannot expect  $\gamma_i$  to remain the same as at RHIC. It has been found that the nuclear modification factor  $R_{AA}$  for Pb-Pb collisions at 2.76 TeV at 0-5% centrality decreases rapidly from  $p_T = 2$  GeV/c to a minimum value of 0.13 at  $p_T = 6-7$  GeV/c, after which there is a significant rise, reaching  $R_{AA} \approx 0.4$  for  $p_T > 30$  GeV/c [41]. Such data suggest that jet quenching becomes less severe at higher momentum, so  $\gamma_i$  should decrease as the hard parton momentum increases. Hence, we parametrize  $\gamma_g$  as

$$\gamma_g(q) = \frac{\gamma_0}{1 + q/q_0}, \quad (17)$$

with  $\gamma_0$  and  $q_0$  to be determined by fitting the hadronic spectra in the intermediate  $p_T$  region, and we continue to set  $\gamma_q = \gamma_g/2$  as before. Although the  $p_T$  distributions will not be computed until Sec. VI after several other issues are discussed, we give here the values  $\gamma_0 = 0.8$  and  $q_0 = 10$  GeV/c that will be determined there, so that our present discussion can proceed with concrete numerical specificity to show the nature of physics involved. Furthermore, we shall hereafter be concerned with only the most central collisions 0-5%. We shall therefore omit the symbol  $b$  and perform all calculation with the appropriate range

of impact parameter. Defining  $\hat{F}_i(q)$  as the average of  $\bar{F}_i(q, \phi)$  over  $\phi$

$$\hat{F}_i(q) = \frac{1}{2\pi} \int_0^{2\pi} d\phi \bar{F}_i(q, \phi), \quad (18)$$

we can, using Eqs. (12-15) and following the details discussed in Refs. [12, 14], compute  $\hat{F}_i(q)$  for all parton types  $i$  listed in Table I, and for all  $q < 30$  GeV/c. Although the hadron transverse momentum  $p_T$  will not exceed 20 GeV/c in our calculation, so that  $p_2$  in Eqs. (1) and (2) is also less than that upper limit, it is necessary to consider higher values of  $q$  because of the integration in Eq. (7). In Fig. 4(a) we show  $\hat{F}_g$  for gluon by the solid line, and in (b)  $\hat{F}_i$  for  $i = q, \bar{q}$  and  $s$  by other line types, assuming that  $\gamma_s = \gamma_q$ , where the subscript  $q$  denotes any of the light quarks. They are compared to  $q^2 f_{g,q}(q)$  for no momentum degradation (i.e.,  $\xi = 0$ ) shown by the lines of open symbols. We recall that  $f_i(k)$  is the initial parton distribution defined in the phase space  $kdk$ , while  $\hat{F}_i(q)$  is the invariant distribution in  $dq/q$ . It is possible to see from Fig. 4 that the ratio  $\hat{F}_i(q)/q^2 f_i(q)$  increases with increasing  $q$ . That is a consequence of  $\gamma_g(q)$  decreasing with  $q$ , as indicated in Eq. (17).

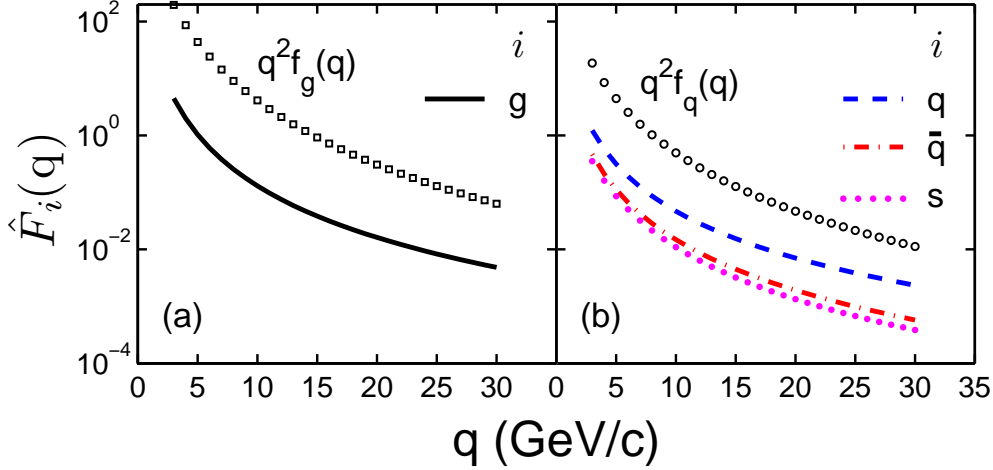


FIG. 4: (Color online) Distribution of minijets at medium surface for 0-5% centrality. Index  $i$  denotes the parton type: (a)  $i = g$  for gluon, (b)  $i = q, \bar{q}, s$  (with  $\bar{s}$  being treated the same as  $s$ ). The line with open squares in (a) represents the distribution of gluons without momentum degradation; the line with open circles in (b) represents the same for light quarks.

$i$	$\hat{A}_i$	$n_i$	$T_i$ [GeV/c]
$g$	8232	3.07	0.092
$u$	6352	2.77	0.051
$d$	8090	2.75	0.048
$\bar{u}$	437	3.04	0.116
$\bar{d}$	407	3.05	0.118
$s, \bar{s}$	133	3.16	0.172

TABLE II: Parameters for  $\hat{F}_i(q)$  in Eq. (19).

For the application of  $\hat{F}_i(q)$  in subsequent calculation, notably in Eq. (7), it is convenient to have an explicit formula. We have been able to fit  $\hat{F}_i(q)$  very well for all  $i$  by use the Tsallis distribution [42]

$$\hat{F}_i(q) = \hat{A}_i \left(1 + \frac{q}{n_i T_i}\right)^{-n_i}, \quad (19)$$

where  $\hat{A}_i$ ,  $n_i$  and  $T_i$  parameters are given in Table II.

With  $\hat{F}_i(q)$  now known explicitly, we can proceed to the calculation of  $\mathcal{S}^j(p_2)$  in Eq. (7). The SPDs  $S_i^j(p_2, q)$  are derived in Refs. [27] and summarized in [14]. Since the fragmentation of hard and semihard partons into shower partons takes place outside the medium in our treatment, the structure of SPDs is independent of the collision energy. Thus  $\mathcal{S}^j(p_2)$  at LHC differs from that at RHIC only because  $\hat{F}_i(q)$  is now enhanced, not because of any changes in  $S_i^j(p_2, q)$ . While  $i$  in Eq. (7) is summed over all parton types listed in Table II,  $j$  will only be  $u$ ,  $d$ ,  $s$  and their antiquarks because in our formalism of recombination gluons do not directly participate in hadronization. They are always converted to  $q\bar{q}$  pairs first, which dress themselves before becoming the constituent quarks of the produced hadrons [30]. The conversion of gluons to  $q\bar{q}$  pairs are referred to as enhancing the sea for hadronization at large rapidity [30, 32]. Here at large  $p_T$  the same concept of gluon conversion applies, except that instead of enhancing the sea each  $q$  and  $\bar{q}$  can participate in forming a hadron, but in single-particle inclusive distribution only the leading partons with large momentum fractions are considered in the calculation.

Before showing the result from calculating  $\mathcal{S}^j(p_2)$ , we note that in using Eq. (7) in practice, apart from  $q$  being integrated from  $q = 2$  to 30 GeV/c, as mentioned earlier, the SPD  $S_i^j(p_2, q)$  is made to deviate from the scaling form  $S_i^j(z)$  by our insertion of a cutoff factor

$c_2(p_2)$

$$S_i^j(p_2, q) = S_i^j(p_2/q) c_2(p_2), \quad (20)$$

where

$$c_2(p_2) = 1 - e^{-(p_2/p_c)^2}, \quad p_c = 0.5 \text{ GeV}/c. \quad (21)$$

Such a factor is necessary to render the shower partons meaningful in the soft region, for otherwise the IR divergent FF,  $D_i(p_T/q)$ , as  $p_T \rightarrow 0$ , would lead to unrealistically large  $S_i^j(p_2/q)$ . This point is discussed in Appendix C of Ref. [14], where  $c_2(p_2)$  is denoted by  $\gamma_2(p_2)$ . The value of  $p_c$  in Eq. (21) is chosen so that we can obtain a good fit of the proton spectrum at low  $p_T$ , as will be shown in Sec. VI. The situation here for LHC is different from that at RHIC, where the shower parton are less important than the thermal partons at low  $p_2$ , so the precise value of  $p_c$  is not significant. At LHC  $\mathcal{S}^j(p_2)$  is dominant throughout all  $p_2$  so without the cutoff  $p_c$  the divergence of  $S_i^j(p_2/q)$  as  $p_2 \rightarrow 0$  would lead to unrealistically large hadronic distribution for  $p_T < 1 \text{ GeV}/c$ . By relinquishing our claim for any reliability of our model predictions in the region  $p_T < 1 \text{ GeV}/c$ , we find that what we can calculate at  $p_T > 1 \text{ GeV}/c$  is insensitive to the precise value of  $p_c$ . We use  $p_c = 0.5 \text{ GeV}/c$  just to fit the proton spectrum at  $p_T < 1 \text{ GeV}/c$ . Note that we use the proton distribution as the guide, not pion, because there are resonance and other contributions to the pion distribution at very low  $p_T$ . The details will become more clear when the mathematical expressions for recombination are shown explicitly below.

Substituting Eqs. (20) and (21) into (7), we obtain the invariant shower-parton distribution  $\mathcal{S}^j(p_2)$  after integrating over  $q$  and summing over all initiating partons  $i$ . For  $j = u$ , it is shown in Fig. 5 by the solid (red) line, plotted against  $p_2$  but labeled as  $p_1$ , since it is to be compared to the thermal parton distribution  $\mathcal{T}(p_1)$  in the same figure. For  $\mathcal{T}(p_1)$  we use Eq. (6) with parameters  $C$  and  $T$  essentially the same as at RHIC, the details of which will be discussed in Sec. VI. The  $\mathcal{T}(p_1)$  distribution is shown by the dashed (blue) line in Fig. 5. Evidently,  $\mathcal{S}(p_1)$  dominates over  $\mathcal{T}(p_1)$  for all  $p_1 > 0.5 \text{ GeV}/c$ . Hereafter, for the sake of brevity we omit the superscript of quark type  $j$  in  $\mathcal{S}^j(p_1)$ , as we routinely do for  $\mathcal{T}(p_1)$ , when no confusion is likely to ensue. This is the most remarkable feature about the parton distribution at LHC. Although we cannot show the phenomenology based on these distribution until later, the dominance of  $\mathcal{S}(p_1)$  is so important that it reorients our thinking about



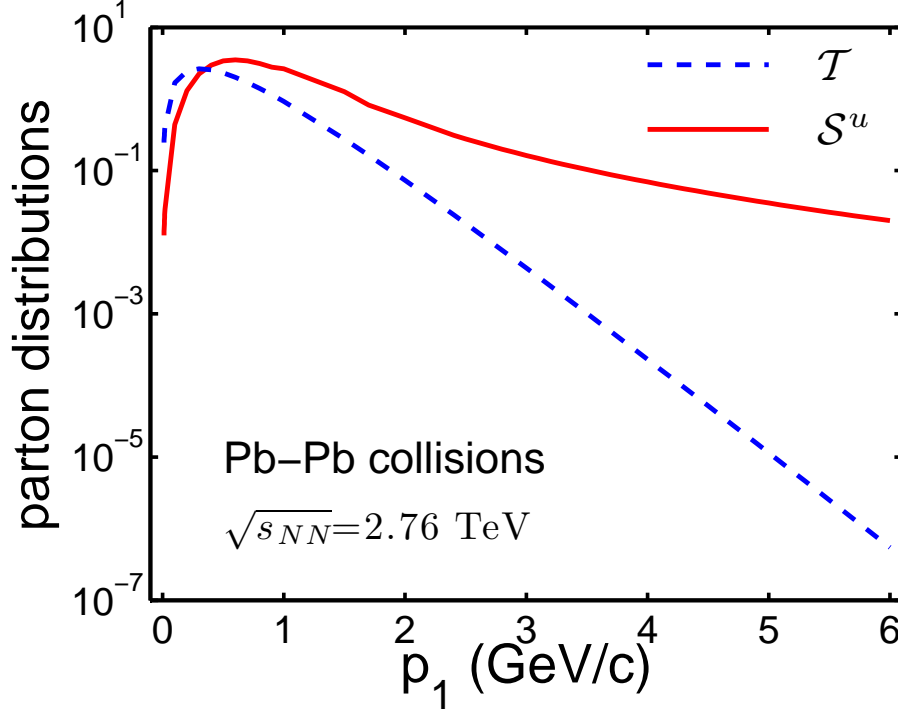


FIG. 5: (Color online) Thermal distribution  $\mathcal{T}(p_1)$  is depicted by the dashed (blue) line for  $T = 0.31$  GeV. Shower parton distribution  $\mathcal{S}^u$  is shown in solid (red) line with low- $p_1$  cutoff.

hadron production at low and intermediate  $p_T$  from this point of our discussion onward. In essence, minijets are so copiously produced at LHC that their effects at low  $p_T$  cannot be ignored, thus posing a substantive question on the meaningfulness of any hydrodynamical study without taking minijets into account.

To place Fig. 5 in the proper context, we show the ratio  $\mathcal{S}/\mathcal{T}$  by the solid line in Fig. 6(a). It is substantially above 1 for  $p_1 > 0.5$  GeV/c. For comparison the ratio for the partons at RHIC is shown by the dashed line in the same figure. Some aspects of the shower partons at RHIC are discussed in Appendix A. We see in Fig. 6(a) that  $\mathcal{S}/\mathcal{T}$  at LHC is significantly larger than that at RHIC. Whereas the latter does not exceed 1 until  $p_1$  is above 2 GeV/c, the former is almost always greater than 1. Since  $\mathcal{T}$  is the same in both, the ratio of  $\mathcal{S}/\mathcal{T}$  at LHC to that at RHIC is just  $\mathcal{S}^{\text{LHC}}/\mathcal{S}^{\text{RHIC}}$ , which is shown in Fig. 6(b), exhibiting a factor of 7 even at  $p_1 \approx 1$  GeV/c. It is therefore reasonable to draw a connection between the enhancement of shower partons and the increase of average multiplicity in Fig. 1 in going from RHIC to LHC energies.

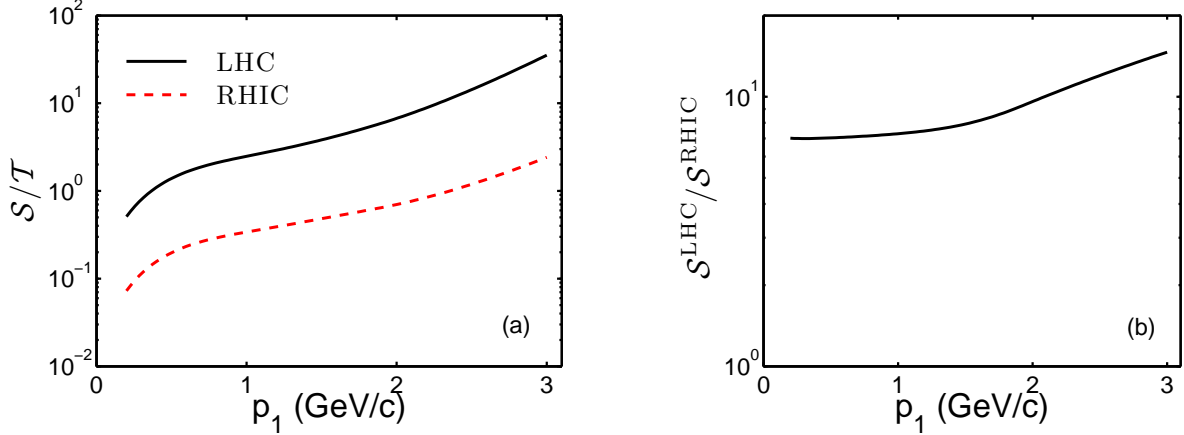


FIG. 6: (Color online) (a) The ratios of  $S/T$  for LHC and RHIC at 0-5% centrality. (b) The ratio of shower-parton distribution at LHC to that at RHIC.

## V. TWO-JET RECOMBINATION

Before we embark on the actual task of computing the inclusive distributions, we discuss an issue that should arise upon examining Fig. 5. We see in that figure that  $\mathcal{S}$  is larger than  $\mathcal{T}$  for all  $p_1 > 0.5$  GeV/c so one would expect the last terms  $\mathcal{SS}$  and  $\mathcal{SSS}$  in Eqs. (4) and (5) to be more important. However, those equations display only the schematic structure of the various components, and are adequate only as a general layout for use in Eqs. (1) and (2). Kinematic constraints on the shower-parton momenta that will be shown in detail in the next section result in the contribution from  $\mathcal{SS}$  and  $\mathcal{SSS}$  terms to be dominant only in the large  $p_T$  region. There is another type of shower-parton recombination that has not been discussed above; that is the subject of our consideration in this section.

In Refs. [11, 13, 14] where SS recombination is considered, the shower partons arise from the same jet. (The same applies to SSS for baryons as well, but will not be reiterated.) Such a term is equivalent to fragmentation, since it is from the FF,  $D_i^\pi(z)$ , that the SPDs are derived in the first place [27]. In view of the dominance of  $\mathcal{S}(p_1)$  over  $\mathcal{T}(p_1)$ , it is reasonable to expect the integral of  $\mathcal{S}(p_1)\mathcal{S}(p_2)$  to be larger than  $\mathcal{T}(p_1)\mathcal{S}(p_2)$  when convoluted with the same RF,  $R^\pi(p_1, p_2, p_T)$ . At this point it is important for us to be more explicit with indices and distinguish one-jet and two-jet recombinations, which we shall denote by  $(\text{SS})^{1j}$  and  $(\text{SS})^{2j}$ , respectively.

In Fig. 7 we show the diagrams in the transverse plane for three types of recombination: (a) TS, (b)  $(\text{SS})^{1j}$  and (c)  $(\text{SS})^{2j}$ . In the notation of Eq. (12),  $k$  is the momentum of the

hard or semihard parton at creation, and  $q$  is the momentum at the medium surface. The thick red vectors have the dual role of representing the jet momentum in the medium and the degradation effect described by  $G(k, q, \xi)$ . The thinner red lines outside the medium are the semihard partons  $q_j$ , which can emit shower partons represented by the thinnest red lines denoted by  $p_j$ . The blue dashed arrows are thermal partons. Recombination is represented by a large black blob with the outgoing open arrow depicting the produced pion. We emphasize that the shower parton lines are inclusive in the sense that only the ones contributing to the formation of the observed hadron are shown. In particular, a gluon generates a cluster of partons which cannot all be depicted. Thus quark types and baryon numbers cannot be recognized from the schematic diagrams. Furthermore, the lengths and angles of the vectors are not drawn to scale due to the limitation in presenting the figures clearly, and should not be taken literally.

Note that in Fig. 7(a) and (b) the hard or semihard partons are labeled by  $i$ , while in (c) the two partons are labeled by  $i$  and  $i'$ . Therein lies the essential point that TS and (SS)<sup>1j</sup> each involves only one jet of type  $i$ , while (SS)<sup>2j</sup> involves two jets of types  $i$  and  $i'$ . Thus for TS and (SS)<sup>1j</sup> there is only one hard scattering contained in  $\hat{F}_i(q)$ , while for (SS)<sup>2j</sup> there are two hard scatterings contained separately in  $\hat{F}_i(q_1)\hat{F}_{i'}(q_2)$ . More explicitly, but leaving out integration over  $q$  and summation over  $i$  for now (with full expression to be shown in the next section), we have

$$\hat{F}_i(q)\widehat{TS}(q, p_T) = \int \frac{dp_1}{p_1} \frac{dp_2}{p_2} \hat{F}_i(q) \mathcal{T}^{\bar{q}}(p_1) S_i^q(p_2, q) R_{q\bar{q}}^\pi(p_1, p_2, p_T), \quad (22)$$

$$\begin{aligned} \hat{F}_i(q)\widehat{SS}(q, p_T) &= \int \frac{dp_1}{p_1} \frac{dp_2}{p_2} \hat{F}_i(q) \{S_i^q(p_1, q), S_i^{\bar{q}}(p_2, q)\} R_{q\bar{q}}^\pi(p_1, p_2, p_T) \\ &= \hat{F}_i(q) \frac{p_T}{q} D_i^\pi(p_T, q), \end{aligned} \quad (23)$$

while for (SS)<sup>2j</sup> we need to retain the  $\phi$  variable in  $\bar{F}_i(q, \phi)$  before it is averaged over  $\phi$  in Eq. (18):

$$\widehat{SS}^{2j} = \int \left[ \prod_{a=1}^2 \frac{dp_a}{p_a} d\phi_a \right] \bar{F}_i(q_1, \phi_1) \bar{F}_{i'}(q_2, \phi_2) S_i^q(p_1, q_1) S_{i'}^{\bar{q}}(p_2, q_2) \mathbf{R}_\Gamma^\pi(p_1, \phi_1, p_2, \phi_2, p_T, \phi). \quad (24)$$

Because there are two initiating hard partons  $i$  and  $i'$  we need to integrate over their respective azimuthal angles  $\phi_1$  and  $\phi_2$ , allowing the RF  $\mathbf{R}_\Gamma^\pi$  to play the role of restricting  $\phi_1$  and  $\phi_2$  to be really equal for the coalescence process to take place. Non-parallel partons have large relative momentum transverse to  $\vec{p}_1 + \vec{p}_2$ , which should not exceed the binding

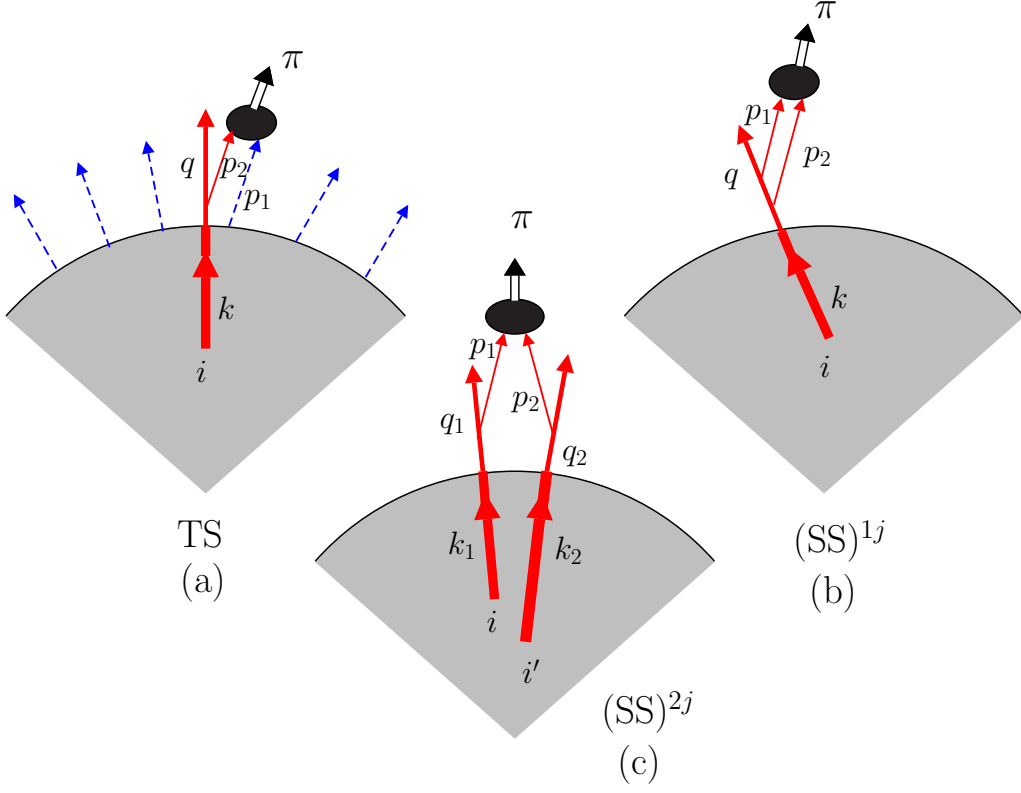


FIG. 7: (Color online) Schematic diagrams for parton recombination of (a) TS, (b) SS in one jet, and (c) SS in two jets. Thick (red) lines represent partons in medium, thin (red) lines partons out of medium, thinnest (red) lines shower partons, and dashed (blue) lines thermal partons. All lines are inclusive in the sense described in the text.

energy of the constituents of the hadron that it is to be formed. That is different from large relative longitudinal momentum parallel to  $\vec{p}_1 + \vec{p}_2$  because in the parton model the momentum fractions of partons in a hadron can vary from 0 to 1 .

The azimuthal angles  $\phi_1$  and  $\phi_2$  may be given by a Gaussian distribution in  $|\phi_1 - \phi_2|$  with an appropriate width. However, since  $\phi_1$  and  $\phi_2$  are integrated over in Eq. (24), it is simpler to adopt a factorizable form that requires the partons to be parallel but with a suitable normalization factor  $\Gamma$  that we can estimate, i.e.,

$$\mathbf{R}_\Gamma^\pi(p_1, \phi_1, p_2, \phi_2, p_T, \phi) = \Gamma \delta(\phi_1 - \phi_2) \delta\left(\frac{\phi_1 + \phi_2}{2} - \phi\right) R^\pi(p_1, p_2, p_T), \quad (25)$$

where  $\Gamma$  is the probability that two parallel partons can recombine. Since the partons are emitted from the medium at early times, we may consider the emitting system as being

a thin almond-shaped overlap region viewed from its side in the same transverse plane at midrapidity as where the pion is detected. For 0-5% centrality the almond is almost circular. The partons at  $\phi_i$  are parallel, but can be emitted at any distance from the center of the circle. Looking at the emitting source edgewise, it is essentially a one-dimensional system of width approximately 10 fm, which is slightly less than  $2R_A$  since high-density partons are not likely to be emitted tangentially from the edges. The two parallel partons should be separated by a distance not greater than the diameter of a pion ( $\sim 1$  fm), given that the jets have some width. Thus our estimate for  $\Gamma$  is the ratio  $\sim 1/10$ . We do not see that any more elaborate analysis of the coalescence process can provide a more transparent description of  $\mathbf{R}_F^\pi$ . Applying Eq. (24) to (23) we obtain upon averaging over  $\phi$

$$\widehat{\mathcal{SS}}^{2j} = \Gamma \int \frac{dp_1}{p_1} \frac{dp_2}{p_2} \hat{F}_i(q_1) S_i^q(p_1, q_1) \hat{F}_{i'}(q_2) S_{i'}^{\bar{q}}(p_2, q_2) R^\pi(p_1, p_2, p_T). \quad (26)$$

By comparing this equation with Eq. (22) we see that the 2j contribution has an extra factor of  $\Gamma \hat{F}_i(q_2)$  with  $p_2$  ranging from 0 to  $q_2$ . On the other hand, the symmetrization of the two shower-parton product in the 1j contribution, when expressed in terms of momentum fractions  $x_i = p_i/q$ , reveals the ranges  $0 < x_2 < 1 - x_1$ , and  $0 < x_1 < 1 - x_2$  in the two terms

$$\{S_i(x_1), S_i(x_2)\} = \frac{1}{2} \left[ S_i(x_1) S_i\left(\frac{x_2}{1-x_1}\right) + S_i(x_2) S_i\left(\frac{x_1}{1-x_2}\right) \right]. \quad (27)$$

Thus, when two shower partons are in the same jet, the sum of their momenta,  $p_1 + p_2$ , cannot exceed the jet momentum  $q$ . That is the kinematical restriction mentioned in the beginning of this section, and corresponds to the familiar condition that  $p_T < q$  in the FF  $D_i^\pi(p_T, q)$  in Eq. (22).

Since the large- $q$  dependence of  $\hat{F}_i(q)$  is power-law behaved, as given explicitly in Eq. (19), the  $(\mathcal{SS})^{1j}$  component dominates at high  $p_T$ , where the components involving the thermal partons (i.e. TT and TS) are damped due to the exponential behavior of  $\mathcal{T}(p_1)$ . The  $(\mathcal{SS})^{2j}$  component involves  $\hat{F}_i(q_1)$  and  $\hat{F}_{i'}(q_2)$  in Eq. (26) so it is suppressed compared to  $(\mathcal{SS})^{1j}$ , but by how much requires explicit calculation.

To take multi-jet recombination into account for the production of proton, we show more explicitly the terms in Eq. (5), but still symbolically,

$$F_{qq} = \mathcal{T}\mathcal{T}\mathcal{T} + \mathcal{T}\mathcal{T}\mathcal{S} + \mathcal{T}(\mathcal{SS})^{1j} + (\mathcal{SSS})^{1j} + \mathcal{T}(\mathcal{SS})^{2j} + [(\mathcal{SS})^{1j}\mathcal{S}]^{2j} + (\mathcal{SSS})^{3j} \quad (28)$$

Except for the first term that does not involve any S, the other six terms are depicted by the six figures in Fig. 8, respectively. The first three figures have only 1-jet and are conventional.

Figure 8 (d) corresponds to Eq. (26) plus one thermal parton, so the equation for it is

$$\mathcal{T}(\widehat{SS})^{2j} = \Gamma \int \frac{dp_1}{p_1} \frac{dp_2}{p_2} \frac{dp_3}{p_3} \mathcal{T}(p_1) \hat{F}_i(q_2) S_i^q(p_2, q_2) \hat{F}_{i'}(q_3) S_{i'}^{q'}(p_3, q_3) R^p(p_1, p_2, p_3, p_T). \quad (29)$$

The last two figures can easily be obtained by straightforward generalization

$$(\widehat{SSS})^{2j} = \Gamma \int \left[ \prod_{a=1}^3 \frac{dp_a}{p_a} \right] \hat{F}_i(q_1) \{S_i^q(p_1, q_1), S_i^{q'}(p_2, q_1)\} \\ \times \hat{F}_{i'}(q_2) S_{i'}^{q''}(p_3, q_2) R^p(p_1, p_2, p_3, p_T), \quad (30)$$

$$(\widehat{SSS})^{3j} = \Gamma^2 \int \left[ \prod_{a=1}^3 \frac{dp_a}{p_a} \hat{F}_{i_a}(q_a) S_{i_a}^{q_a}(p_a, q_a) \right] R^p(p_1, p_2, p_3, p_T). \quad (31)$$

Three-jet recombination is highly suppressed and will be neglected in the following.

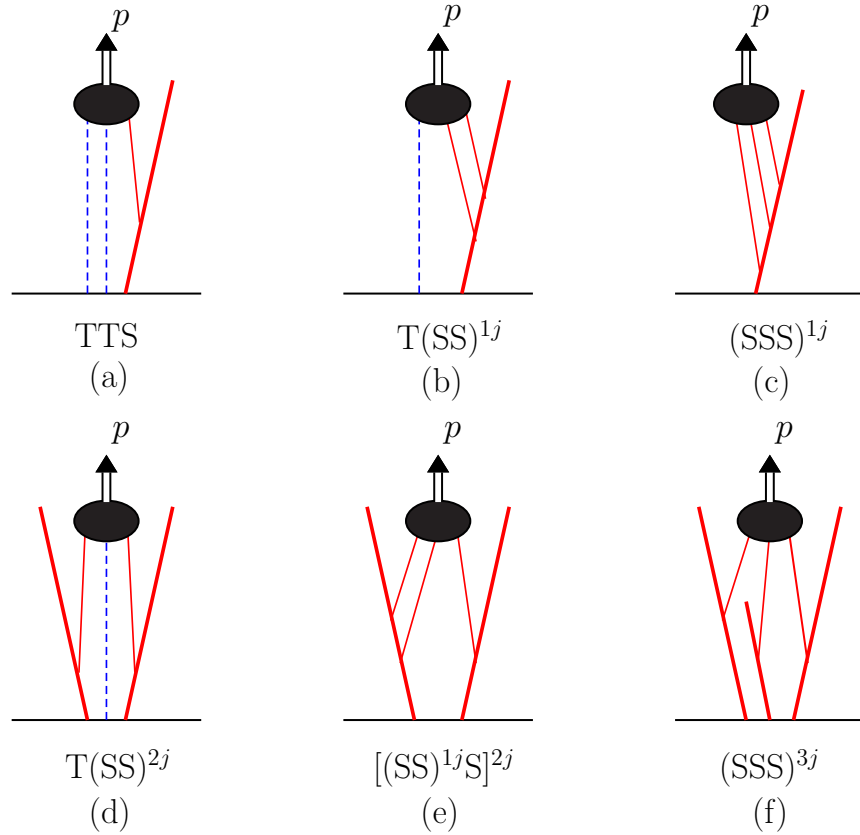


FIG. 8: (Color online) Diagrams showing the inclusive processes for proton production by recombination of partons with same line-types as in Fig. 7.

## VI. TRANSVERSE MOMENTUM DISTRIBUTIONS OF HADRONS

We now calculate the  $p_T$  distributions of  $\pi, p, K$  and  $\Lambda$  produced at  $\eta \sim 0$  and for 0-5% centrality in Pb-Pb collisions at 2.76 TeV. They are based on the essential points discussed

in the preceding sections, some of which have previously been applied to collisions at RHIC [11, 14]. Now we consider LHC without changing the basic formalism. Although we have studied the  $p_T$  spectra at LHC before [13], it was, however, for a limited range of  $p_T$  ( $< 5$  GeV/c) and was based on a simple assumption about momentum degradation, which we have subsequently found to be unrealistic as the  $p_T$  range is extended to above 10 GeV/c. Our present treatment of momentum degradation, discussed in Sec. IV, enables us below to reproduce the data up to  $p_T \sim 20$  GeV/c, thus superseding the earlier parametrizations in [13]. Nevertheless, we stress by repeating that the basic equations are the same, as summarized in [14], except that a new  $\gamma_g$  is to be adjusted to fit the data.

### A. Pion and proton production

To be specific we consider the production of  $\pi^+$

$$\frac{dN_\pi^{TT}}{p_T dp_T} = \frac{C^2}{6} e^{-p_T/T}, \quad (32)$$

$$\frac{dN_\pi^{TS}}{p_T dp_T} = \frac{C}{p_T^3} \int_0^{p_T} dp_1 p_1 e^{-p_1/T} \left[ \mathcal{S}^u(p_T - p_1) + \mathcal{S}^{\bar{d}}(p_T - p_1) \right], \quad (33)$$

$$\frac{dN_\pi^{SS^{1j}}}{p_T dp_T} = \frac{1}{p_T} \int \frac{dq}{q^2} \sum_i \hat{F}_i(q) D_i^\pi(p_T, q), \quad (34)$$

$$\frac{dN_\pi^{SS^{2j}}}{p_T dp_T} = \frac{\Gamma}{p_T^3} \int_0^{p_T} dp_1 \mathcal{S}^u(p_1) \mathcal{S}^{\bar{d}}(p_T - p_1). \quad (35)$$

While pion mass is neglected above, proton mass is certainly not negligible, so  $p^0$  in Eq. (2) becomes the transverse mass  $m_T^p = (m_p^2 + p_T^2)^{1/2}$  for  $\eta = 0$ . With the RF given in Eq. (9), we have

$$\frac{dN_p^{TTT}}{p_T dp_T} = g_{st}^p g_p g'_p \frac{C^3 p_T^2}{m_T^p} e^{-p_T/T}, \quad (36)$$

where  $g'_p = B(\alpha + 2, \beta + 2)B(\alpha + 2, \alpha + \beta + 4)$ ,  $\alpha$  and  $\beta$  being given after Eq. (9), and

$$\begin{aligned} \frac{dN_p^{TTS}}{p_T dp_T} = & \frac{g_{st}^p g_p C^2}{m_T^p p_T^{2\alpha+\beta+3}} \int_0^{p_T} dp_1 \int_0^{p_T-p_1} dp_2 e^{-(p_1+p_2)/T} \\ & \times \left\{ (p_1 p_2)^{\alpha+1} (p_T - p_1 - p_2)^\beta \mathcal{S}^d(p_T - p_1 - p_2) \right. \\ & \left. + p_1^{\alpha+1} p_2^{\beta+1} (p_T - p_1 - p_2)^\alpha \mathcal{S}^u(p_T - p_1 - p_2) \right\}, \end{aligned} \quad (37)$$

$$\begin{aligned}
\frac{dN_p^{TSS^{1j}}}{p_T dp_T} &= \frac{g_{st}^p g_p C}{m_T^p p_T^{2\alpha+\beta+3}} \int_0^{p_T} dp_1 \int_0^{p_T-p_1} dp_2 e^{-p_1/T} \\
&\times \left\{ p_1^{\beta+1} p_2^\alpha (p_T - p_1 - p_2)^\alpha \mathcal{S}^{uu}(p_2, p_T - p_1 - p_2) \right. \\
&\left. + p_1 (p_1 p_2)^\alpha (p_T - p_1 - p_2)^\beta \mathcal{S}^{ud}(p_2, p_T - p_1 - p_2) \right\}, \quad (38)
\end{aligned}$$

$$\frac{dN_p^{SSS^{1j}}}{p_T dp_T} = \frac{1}{m_p^T} \int \frac{dq}{q^2} \sum_i \hat{F}_i(q) D_i^p(p_T, q), \quad (39)$$

where  $\mathcal{S}^{qq}$  in Eq. (38) is

$$\mathcal{S}^{qq}(p_2, p_3) = \int \frac{dq}{q} \sum_i \hat{F}_i(q) S_i^q(p_2, q) S_i^q(p_3, q - p_2). \quad (40)$$

Equations (37)-(39) correspond to Fig. 8(a)-(c). For 2-jet contributions in Fig. 8(d) and (e) we have

$$\begin{aligned}
\frac{dN_p^{TSS^{2j}}}{p_T dp_T} &= \frac{g_{st}^p g_p C \Gamma}{m_T^p p_T^{2\alpha+\beta+3}} \int_0^{p_T} dp_1 \int_0^{p_T-p_1} dp_2 e^{-p_1/T} \\
&\times \left\{ p_1^{\beta+1} p_2^\alpha (p_T - p_1 - p_2)^\alpha \mathcal{S}^u(p_2) \mathcal{S}^u(p_T - p_1 - p_2) \right. \\
&\left. + p_1 (p_1 p_2)^\alpha (p_T - p_1 - p_2)^\beta \mathcal{S}^u(p_2) \mathcal{S}^d(p_T - p_1 - p_2) \right\}, \quad (41)
\end{aligned}$$

$$\begin{aligned}
\frac{dN_p^{SSS^{2j}}}{p_T dp_T} &= \frac{g_{st}^p g_p \Gamma}{m_T^p p_T^{2\alpha+\beta+3}} \int_0^{p_T} dp_1 \int_0^{p_T-p_1} dp_2 \\
&\times \left\{ p_1^\beta p_2^\alpha (p_T - p_1 - p_2)^\alpha \mathcal{S}^d(p_1) \mathcal{S}^{uu}(p_2, p_T - p_1 - p_2) \right. \\
&\left. + (p_1 p_2)^\alpha (p_T - p_1 - p_2)^\beta \mathcal{S}^u(p_1) \mathcal{S}^{ud}(p_2, p_T - p_1 - p_2) \right\}. \quad (42)
\end{aligned}$$

The above equations describe the production of pion and proton in the recombination model for hadronization at the final stage of the nuclear collision process where the medium density is low. Since thermal partons represent the properties of the bulk medium at hadronization irrespective of the initiating system, we use for the normalization factor  $C$  and inverse slope  $T$  in Eq. (6) the same values as at RHIC [11]

$$C = 23.2 \text{ GeV}^{-1}, \quad T = 0.31 \text{ GeV}. \quad (43)$$



To justify the use of these values for collisions at LHC, we recall first that in our treatment of hadronization the thermal distributions  $\mathcal{T}(p_1)$  is not what can be derived from hydro studies. At RHIC it is determined by fitting the pion distribution at  $p_T < 2$  GeV/c. Using Eqs. (6) and (8) in (1) one obtains (32) for TT recombination only, which yields the values of  $C$  and  $T$  in Eq. (43) in order to reproduce the pion data at low  $p_T$  [11], as can be seen in Fig. 17 in Appendix A below. As mentioned earlier in Sec. III, the thermal partons include the soft partons generated by hard and semihard partons as they traverse the medium and have thermalized with the bulk partons by the end of the deconfined phase. When those thermal partons are dilute enough and be ready for confinement through recombination, their local properties are no longer sensitive to the collisional system in which the medium is created initially. The concept is consistent with the notion of universal hadrosynthesis where statistical study of hadron ratios has found universality independent of collision energy, analogous to water vapor condensing at 100°C independent of how hot it has previously been.  $C$  and  $T$  are local measures that carry no information of the global properties, such as rapidity range and overall multiplicities, which depend on the collision energy. The distributions we study are at mid-rapidity, so the increase of total multiplicity due largely to the broadening of the rapidity plateau is not of concern here. Our interest is in the increase of  $dN/d\eta|_{\eta \sim 0}$  which we claim is related to the increase of  $\mathcal{S}^q(p_2)$  by demonstrating that the observed spectra can be reproduced in the RM. The thermal distribution  $\mathcal{T}(p_1)$  was determined at RHIC for low  $p_1$  where  $\mathcal{S}(p_2)$  is negligible; that same  $\mathcal{T}(p_1)$  is now used at LHC. In Appendix B it is shown that the use of any values of  $C$  and  $T$  different from Eq. (43) fails to reproduce the data at all  $p_T$ . We remark, parenthetically, that the value of  $C$  above corresponds very well to the formula in Ref. [14] that gives the centrality dependence

$$C(N_{\text{part}}) = 3.43 N_{\text{part}}^{0.32}, \quad (44)$$

wherein we use  $N_{\text{part}} = 383$  for 0-5% in Pb-Pb collisions [43].

It is reasonable to question why  $C$  should remain the same as at RHIC, when more partons are produced at LHC, even though  $T$  is the same at hadronization. Our answer is that our formalism is inadequate to treat accurately the hadron formation at very low  $p_T$  for  $p_T < 1$  GeV/c. The values of  $C$  and  $T$  in Eq. (43) are used for calculating the spectra for  $p_T > 1$  GeV/c. At lower  $p_T$  our pion distribution is lower than the data, which is undoubtedly related to the extra low- $p_1$  partons created at LHC that we cannot easily include in our

parametrization. Besides, there are resonance contribution to the pion spectrum that we have not counted for.

We recall that in order to tame the soft shower parton distributions from minijets we need to introduce a cut-off parameter  $p_c$  in the SPD  $S_i^j(p_2, q)$  in Eq. (19). The value of  $p_c$  is determined mainly by keeping the proton distribution under bound for  $p_T < 1$  GeV/c, since pions have resonance and other contributions mentioned above that are not included in Eqs. (32)-(34). Nevertheless, the dependence on  $p_c$  is not sensitive; its value at 0.5 GeV/c is essentially chosen as a reasonable value. Such a cutoff in the shower parton  $\mathcal{S}^q(p_3)$  for  $p_3 < 0.5$  GeV/c cannot affect the outcome of the dominant TTS contribution in the  $1 < p_T < 5$  GeV/c (to be seen in Fig. 10 below) because at small  $p_3$  we see in Eq. (37) that  $p_1 + p_2 = p_T - p_3$  must be greater than 0.5 GeV/c so the integral is suppressed by the exponential factor  $e^{-(p_1+p_2)/T}$  in the integrand.

The other parameters  $\gamma_0$  and  $q_0$  in Eq. (17) for the  $q$ -dependent gluon degradation factor  $\gamma_g(q)$  are crucial in our attempt to find a good fit of both  $\pi$  and  $p$  distributions at all  $p_T$  up to 20 GeV/c. That makes good sense in physics since the degradation of hard- and semihard-parton momenta is the central theme of heavy-ion physics at LHC. Our study here reveals how important minijets are in explaining the hadron spectra at all  $p_T$  observed. With the choice

$$\gamma_0 = 0.8 \quad \text{and} \quad q_0 = 10 \text{ GeV/c} \quad (45)$$

we calculate the pion distribution for  $0 < p_T < 20$  GeV/c and obtain the different components shown in Fig. 9 by different line types, although only the region  $p_T > 1$  GeV/c is reliable. Their sum in black-cross line agrees with data from ALICE [47] very well for  $p_T > 1$  GeV/c. The solid black line includes what we cannot calculate and is put in by hand to raise the distribution to fit the data at  $p_T < 1$  GeV/c. We note that TS is larger than TT for  $p_T > 1$  GeV/c. The total goes below the data points at  $p_T > 15$  GeV/c. Some further adjustment of  $\gamma_g(q)$  at very high  $q$  can repair that deficiency by raising SS<sup>1j</sup> there, but that much fine tuning is not our interest here since our focus is on the interplay among the different components at low and intermediate  $p_T$ . The 2-jet component SS<sup>2j</sup> is too small to be significant; nevertheless, it is interesting to observe that SS<sup>2j</sup> has very nearly the same magnitude as SS<sup>1j</sup> at  $p_T \approx 2.5$  GeV/c. That is not the situation at RHIC, as can be seen in Fig. 17 in Appendix A, where SS<sup>2j</sup> is much less than SS<sup>1j</sup> at all  $p_T$ . The difference owes

its origin to the relative sizes of  $\mathcal{S}(p_1)$  shown in Fig. 6(a) and (b). Since recombination is dominated by shower partons in the dense region, i.e., at low  $p_1$ , two such partons from nearby jets can contribute as much as from a single jet.

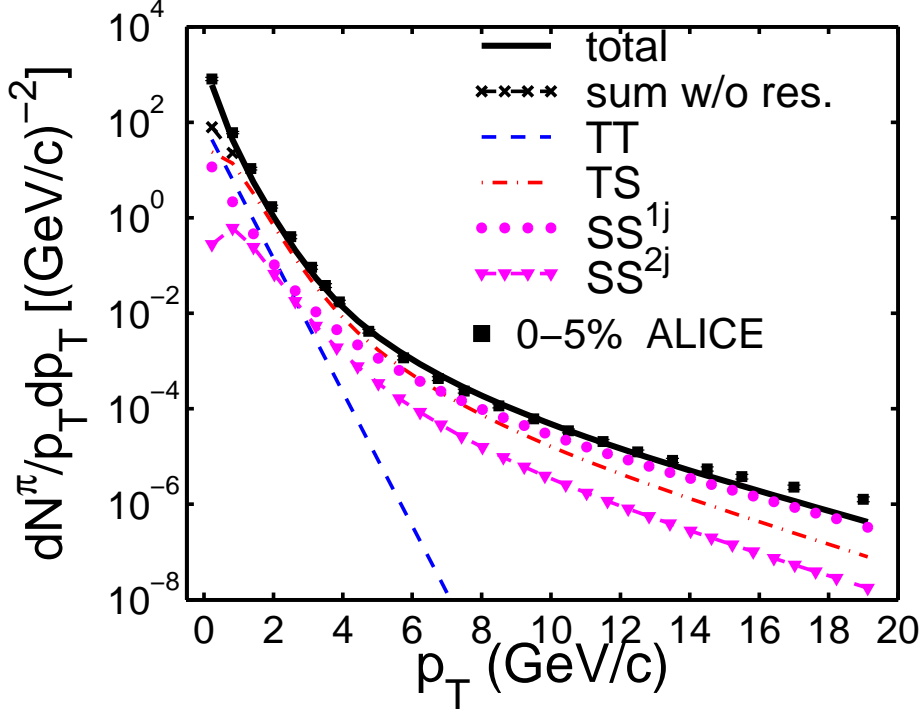


FIG. 9: (Color online) Transverse momentum distribution of pion produced in Pb-Pb collision at  $\sqrt{s_{NN}} = 2.76$  TeV. Data are from [22] for centrality 0-5%.

Without changing any parameter we calculate the proton distribution that is shown in Fig. 10. It also agrees with the data [47] extremely well. Note that TTS, TSS<sup>1j</sup>, TSS<sup>2j</sup> and SSS<sup>1j</sup> components are all of similar magnitudes at  $p_T \approx 6$  GeV/c; together they lift the total to meet the data points. That is a feature that is unique among the hadronization models. As with the pion distribution, TTS is larger than TTT for  $p_T > 1$  GeV/c, demonstrating again that the soft shower partons play an important role at low  $p_T$ . Furthermore, one sees that SSS<sup>2j</sup>  $\approx$  SSS<sup>1j</sup> around  $p_T \approx 3$  GeV/c just as SS<sup>2j</sup>  $\approx$  SS<sup>1j</sup> for pions, although they are all much less than TTS and TS, respectively.

With the results shown in Fig. 9 and 10 we regard our main objective as having been accomplished. It is non-trivial to reproduce the data in such a wide range of  $p_T$  and it is remarkable that the main input that is adjustable is just the momentum degradation factor  $\gamma_g(q)$  in Eq. (17). What we have obtained for  $\gamma_0$  and  $q_0$  in Eq. (45) are good not only for

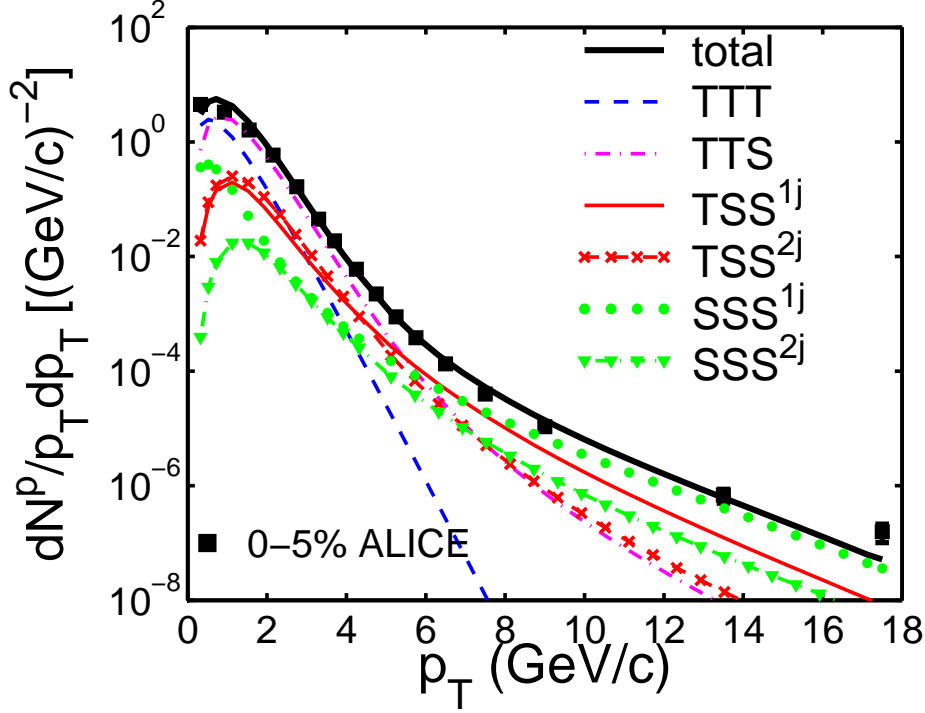


FIG. 10: (Color online) Transverse momentum distribution of proton produced in Pb-Pb collision at  $\sqrt{s_{NN}} = 2.76$  TeV. Data are from [22] for centrality 0-5%.

$\pi$  and  $p$  distributions, but also for all other particles, as we shall show below. Thus the result strongly supports the assertion that minijet production plays the dominate role in the structure of hadronic spectra. The corresponding shower partons have been exhibited already in Fig. 5 together with discussions on their dominance over thermal partons for nearly all  $p_1$ .

### B. $K$ and $\Lambda$ production

Proceeding to the production of strange particles, we use the same formalism as for pion and proton, except that  $s$  quark being more massive than the light quarks requires separate attention. For the thermal  $s$  quarks we use the same distribution as in Eq. (6)

$$\mathcal{T}^s(p_1) = C p_1 e^{-p_1/T_s} \quad (46)$$

but with a different inverse slope  $T_s$ , which is the only parameter we adjust to fit the data. Since the  $s$  quark mass,  $m_s$ , does not appear explicitly in Eq. (46), and also since  $T_s$  may be regarded as an effective temperature at the time of hadronization, the fluid velocity may

raise  $T_s$  above  $T$  (for light quarks). The  $s$  shower parton distribution  $\mathcal{S}^s(p_2)$  is as given in Eq. (7) with the unintegrated SPD  $S_i^j(z)$  determined from the FFs into  $K$  and  $\Lambda$  [11, 46]. The degradation of  $s$ -quark momentum is taken to be the same as others, i.e.,  $\gamma_s = \gamma_q = \gamma_g/2$ .

With the RF for kaon given in Ref. [44, 45] we have for the  $K^+$  distributions

$$\frac{dN_K^{TT}}{p_T dp_T} = \frac{12C^2}{m_T^K p_T^5} \int_0^{p_T} dp_1 p_1 (p_T - p_1)^2 p_1 e^{-p_1/T} (p_T - p_1) e^{-(p_T - p_1)/T_s}, \quad (47)$$

$$\begin{aligned} \frac{dN_K^{TS}}{p_T dp_T} &= \frac{12C}{m_T^K p_T^5} \int_0^{p_T} dp_1 p_1^2 (p_T - p_1)^2 \\ &\times \left[ e^{-p_1/T} \mathcal{S}^{\bar{s}}(p_T - p_1, c) + \left( \frac{p_T}{p_1} - 1 \right) e^{-(p_T - p_1)/T_s} \mathcal{S}^u(p_1) \right], \end{aligned} \quad (48)$$

$$\frac{dN_K^{SS^{1j}}}{p_T dp_T} = \frac{1}{m_T^K} \int \frac{dq}{q^2} \sum_i \hat{F}_i(q) D_i^K(p_T, q), \quad (49)$$

$$\frac{dN_K^{SS^{2j}}}{p_T dp_T} = \frac{12\Gamma}{m_T^K p_T^5} \int_0^{p_T} dp_1 p_1 (p_T - p_1)^2 \mathcal{S}^u(p_1) \mathcal{S}^{\bar{s}}(p_T - p_1). \quad (50)$$

With  $T_s$  being the only adjustable parameter we obtain for

$$T_s = 0.34 \text{ GeV}/c \quad (51)$$

the distribution shown in Fig. 11. Evidently, the data from ALICE [47] are well reproduced. The value of  $T_s$  is slightly higher than  $T$  in Eq. (43). As it is with pions, the TS components is greater than TT for  $p_T > 0.5 \text{ GeV}/c$ . Although  $\mathcal{S}^s(p_1)$  is suppressed relative to  $\mathcal{S}^u(p_1)$ , the  $\bar{s}u$  recombination sustains the TS component. However,  $SS^{1j}$  is clearly much lower than that for pion in Fig. 9 at low  $p_T$ . Note that  $SS^{2j}$  is again very close to  $SS^{1j}$  at  $p_T \approx 2 \text{ GeV}/c$ .

For  $\Lambda$  production we use Eq. (46) again for the thermal  $s$  quarks, but allow  $T_s$  to be different from the value in Eq. (51). Appendix C contains the explicit distributions of the various components. With the choice

$$T_s^\Lambda = 0.42 \text{ GeV}/c \quad (52)$$

we obtain the result shown in Fig. 12. The data [47] are reproduced very well. The physics is clearly very much the same as for  $\pi, p$  and  $K$ . The value of  $T_s^\Lambda$  is higher because  $m_\Lambda$  is higher, although how the thermal partons depend on the quark mass is not specified explicitly. We stress that the momentum degradation parameters have not been adjusted so the hard parton and minijet distributions  $\hat{F}_i(q)$  are the same as described in Sec. IV, independent of the hadrons produced. Thus the recombination model has enabled us to calculate the spectra of all strange and non-strange hadron at all  $p_T$  in a universal formalism.

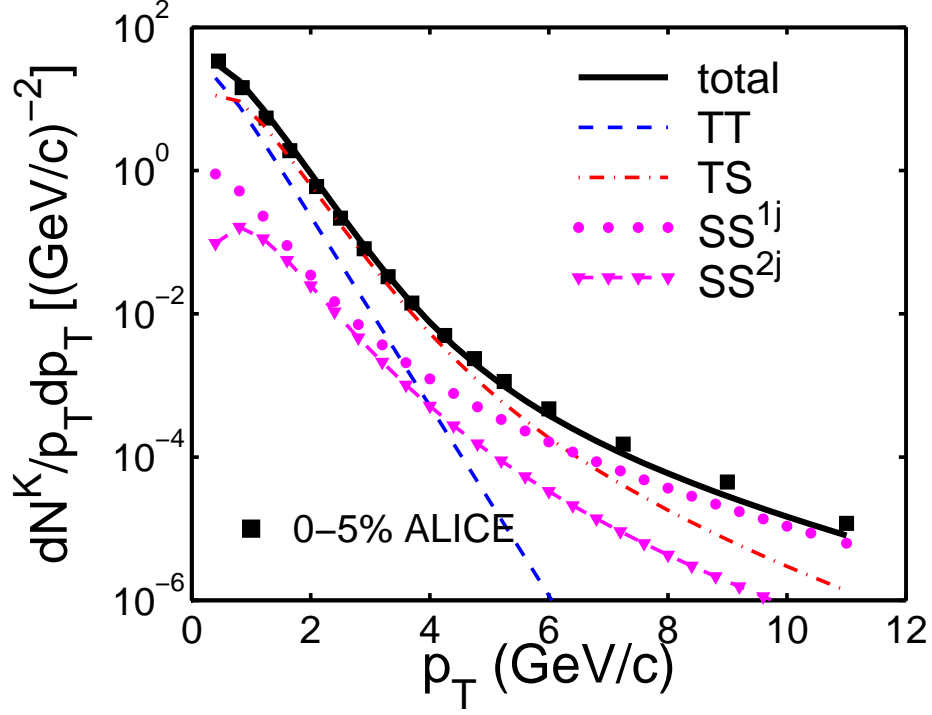


FIG. 11: (Color online) Transverse momentum distribution of kaon produced in Pb-Pb collision at  $\sqrt{s_{NN}} = 2.76$  TeV. Data are from [47] for centrality 0-5%.

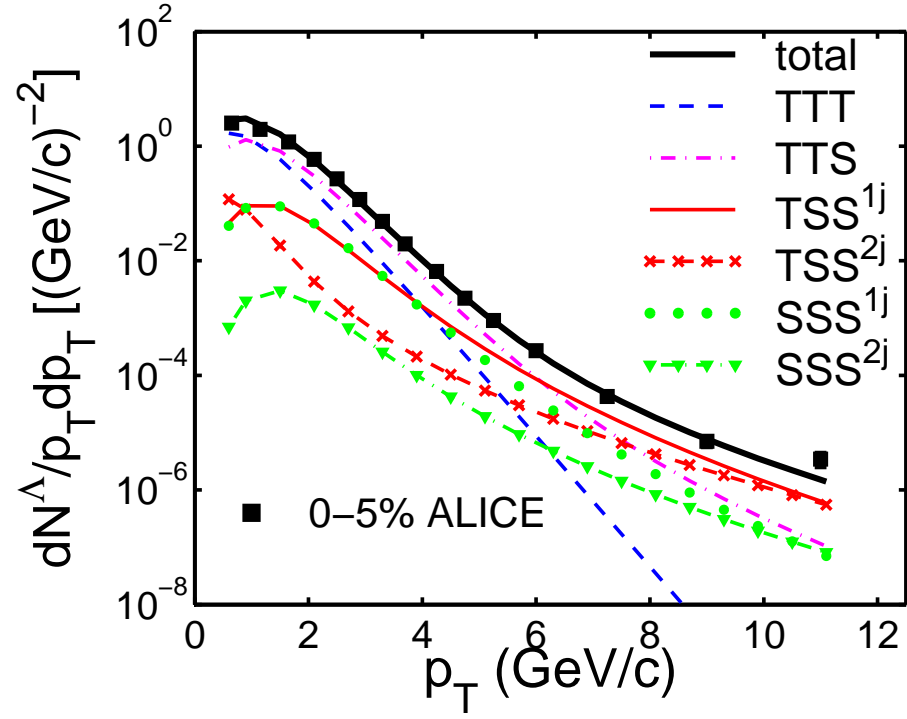


FIG. 12: (Color online) Transverse momentum distribution of  $\Lambda$  produced in Pb-Pb collision at  $\sqrt{s_{NN}} = 2.76$  TeV. Data are from [47] for centrality 0-5%.

## VII. MULTI-STRANGE HYPERONS AND MESON

We complete our investigation of hadron production by considering  $\Xi$ ,  $\Omega$  and  $\phi$ . Apart from different quark contents of those particles, the physics of hadronization through recombination is the same as before. Since they cannot be used either as target on beam particles, their wave functions in terms of momentum fractions of constituent quarks are not known as firmly as we do with  $\pi$ ,  $K$  and  $p$ . Furthermore, there is the question of the probability for more than one strange quark to find one another to recombine. As the system expands, the plasma gets out of chemical equilibrium first as the temperature is lowered because  $gg \rightarrow s\bar{s}$  and  $q\bar{q} \rightarrow s\bar{s}$  processes become less frequent than their reverses on account of  $m_s > m_q > m_g$ . Thus the density of  $s$  quarks becomes lower. The language used above is that of the conventional interpretation of the expanding medium getting out of chemical equilibrium. We need not subscribe to the details of that description, while still adhering to the qualitative physical picture of the system that has general validity. Thus we proceed in the same manner as we have for  $\pi$  and  $p$ . For a single  $s$  quark to hadronize at late time there are abundant light quarks in the neighborhood to form  $K$  and  $\Lambda$  with. However, for multi-strange hadron to form, the probability of  $ss$ ,  $sss$  or  $s\bar{s}$  to be in close proximity of one another at late time is reduced, when the density of  $s$  quark is lower than that of light quarks. If at earlier time  $\Xi$ ,  $\Omega$  and  $\phi$  are formed at higher density, their survival in the medium is suppressed due to their dissociation through interaction with the plasma that is still active. Thus in either case the rate of multi-strange hadron production is lower. We cannot predict that rate in the recombination model, so an adjustable parameter will be used to fit the overall normalization; that is in addition to the inverse slope  $T_s$ , since each particle has its own hadronization time and mass effect on the effective temperature. On the other hand, the density of shower partons arising from hard and semihard partons is independent of the final hadrons formed, so we can still use our formalism to calculate the various components of the  $p_T$  distributions.

The detail equations for  $\Xi$  and  $\Omega$  formations are given in Appendices D and E, respectively. The only free parameters we use in each case are  $g_h$  and  $T_s$ . For best fit we obtain

$$\Xi : \quad g_\Xi = 6 \times 10^{-3}, \quad T_s = 0.46 \text{ GeV}/c, \quad (53)$$

$$\Omega : \quad g_\Omega = 9 \times 10^{-4}, \quad T_s = 0.51 \text{ GeV}/c. \quad (54)$$

The results are shown in Figs. 13 and 14, reproducing the data very well. There are, however, some differences in the strengths of different components, even though the shower partons are the same in all cases.

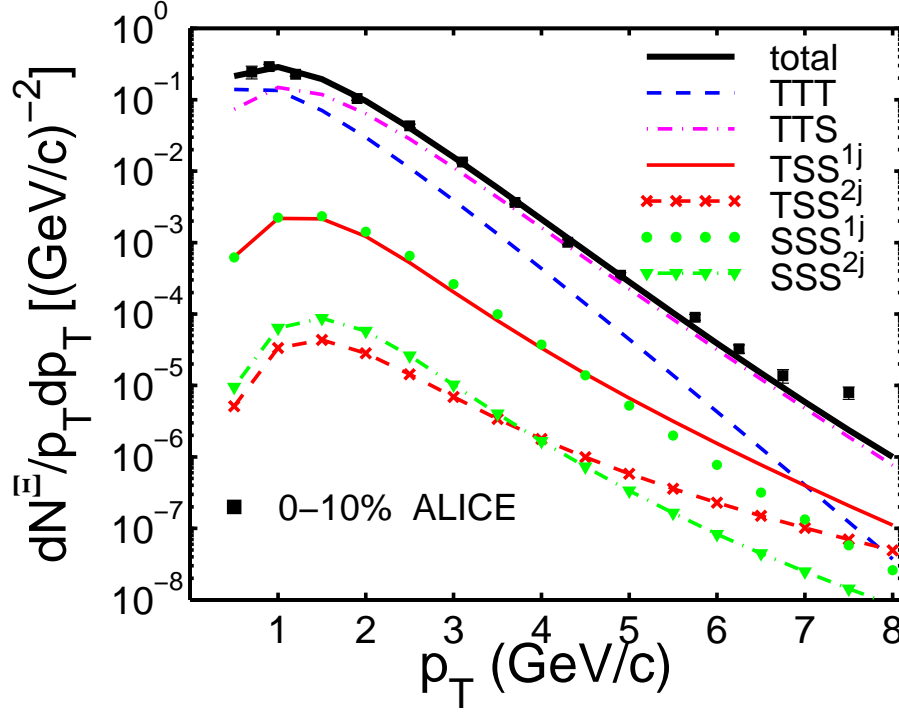


FIG. 13: (Color online) Transverse momentum distribution of  $\Xi$  produced in Pb-Pb collision at  $\sqrt{s_{NN}} = 2.76$  TeV. Data are from [23] for centrality 0-10%.

What is most noticeable about the  $\Xi$  distributions is that the TTS component dominates the whole spectrum for  $p_T > 1$  GeV/c and that TSS and SSS components are much lower. The relative strengths of those components are unlike the situation with proton and  $\Lambda$ . Whereas the S in TTS can be non-strange, TSS must have at least one  $s$  in the SS, and SSS must have two  $s$  quarks. Since  $S^s$  is suppressed compared to  $S^q$ , the ordering of TTS, TSS and SSS is evident in Fig. 13. Moreover,  $TSS^{1j}$  and  $TSS^{2j}$  have roughly the same magnitude; so also do  $SSS^{1j}$  and  $SSS^{2j}$ .

For  $\Omega$  production shown in Fig. 14, similar remarks about the ordering of the various components can be made as for  $\Xi$ . One notable difference is that this time even TTS is suppressed relative to TTT. That is because every coalescing quark for  $\Omega$  must be strange, so  $S^s$  in TTS lowers its magnitude relative to TTT. Herein lies a very interesting point that was noticed several years ago even in RHIC data [48, 49]. The  $p_T$  distribution of  $\Omega$  is exponential



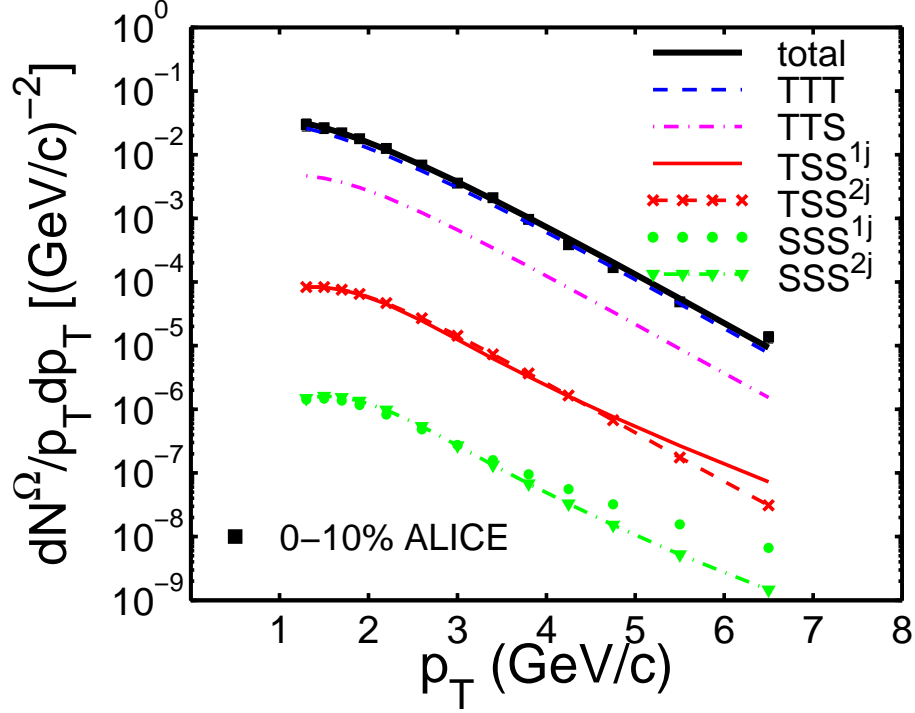


FIG. 14: (Color online) Transverse momentum distribution of  $\Omega$  produced in Pb-Pb collision at  $\sqrt{s_{NN}} = 2.76$  TeV. Data are from [23] for centrality 0-10%.

(apart from the prefactor  $p_T^2/m_T^\Omega$  in Eq. (E1)) without any power-law up-bending at high  $p_T$ . It means that  $\Omega$  is produced thermally even at  $p_T \sim 6$  GeV/c without any contribution from parton fragmentation, which is the usual mechanism considered in pQCD. Neither can hydrodynamics be applied to particle production at such high  $p_T$ . In recombination each  $s$  quark need only be at  $p_T < 2$  GeV/c on the average. Our thermal partons at  $T_s = 0.51$  GeV/c imply that  $\Omega$  is formed earlier than other hyperons. In fact, it is of interest to exhibit the dependence of  $T_s$  on the number  $n_s$  of  $s$ -quark content of the hyperons. Figure 15 shows that there is a linear increase from  $\Lambda$  to  $\Omega$ , and therefore non-linear if plotted against the hyperon masses, since  $m_\Xi - m_\Lambda = 200$  MeV and  $m_\Omega - m_\Xi = 367$  MeV.

A comparison between Figs. 10 and 14 reveals the drastic difference in the compositions of the various components contributing to  $p$  and  $\Omega$ . For  $p$  the all thermal TTT component is unimportant compared to TTS, TSS and SSS, while for  $\Omega$  TTT is the only dominant component. If we were to compare only the TTT components in  $p$  and  $\Omega$ , then their ratio  $(\Omega/p)^{\text{TTT}}$  would be exponentially rising in  $p_T$ . Using  $T = 0.31$  GeV and  $T_s = 0.51$  GeV, that ratio rises by 3 orders of magnitude if only the exponential factors are considered with

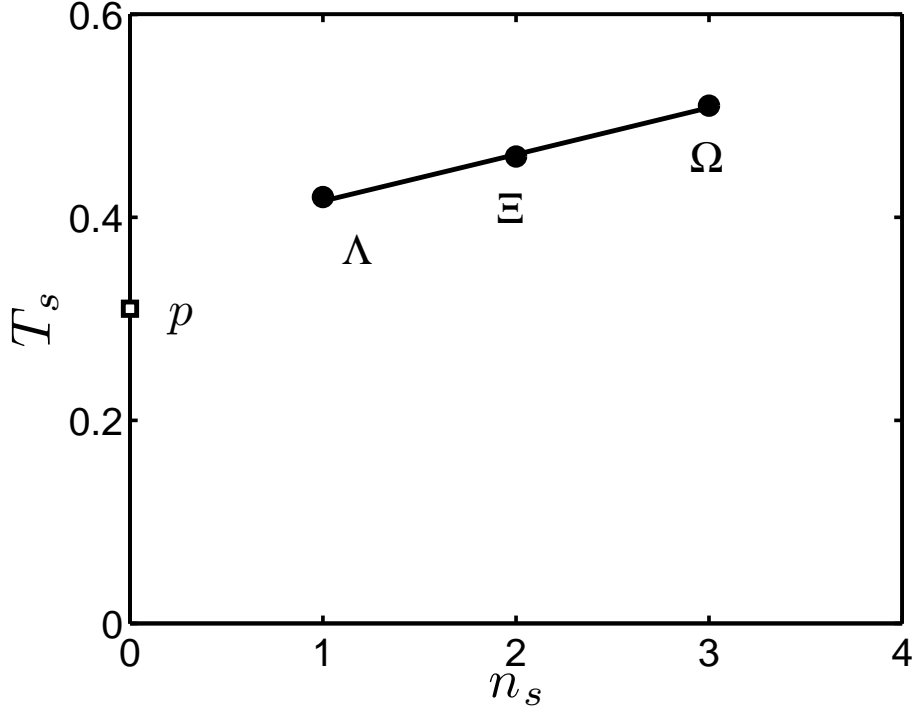


FIG. 15: Linear dependence of  $T_s$  on the number  $n_s$  of strange quarks in hyperons.

neglect of the multiplicative factors. In reality, as we have seen in Fig. 3, the ratio for LHC rises by only a factor of 10. The reason is, of course, the dominance of the  $q$  shower partons in the production of proton, as evident from Fig. 10, where fragmentation is not important until  $p_T > 7$  GeV/c. On the other hand, the  $s$  shower partons are unimportant for the production of  $\Omega$ , which can adequately be described by the exponential behavior of TTT alone. In Fig. 3 we have noted the difference between LHC and RHIC in the  $p_T$  dependencies of  $\Omega/p$ . While  $\Omega$  production at RHIC is also mainly TTT and thus exponential [12, 49], Fig. 18 in Appendix A shows that the  $p_T$  distribution for proton at RHIC has a transition from TTT to TTS in the region  $3 < p_T < 4$  GeV/c. That accounts for the saturation of  $\Omega/p$  in that region in Fig. 3. That transition is absent in Fig. 10 for LHC, hence no saturation seen for LHC in Fig. 3. All these inter-related phenomena can be traced to the simple source, namely:  $q$  shower partons are abundant at LHC, not  $s$  shower partons.

Lastly, we consider the production of  $\phi$ , for which the equations are given in Appendix F. Since no light quarks are involved in the formation of both  $\Omega$  and  $\phi$ , we use the same value of  $T_s$  for both, i.e.,  $T_s = 0.51$  GeV. By varying  $g_\phi$  only for the overall normalization, we obtain the result shown in Fig. 16 for  $g_\phi = 0.07$ . The underlying components are very

similar to those for  $\Omega$ , namely: TT dominates over TS, while SS (whether 1j or 2j) is nearly 2 orders of magnitudes farther down.

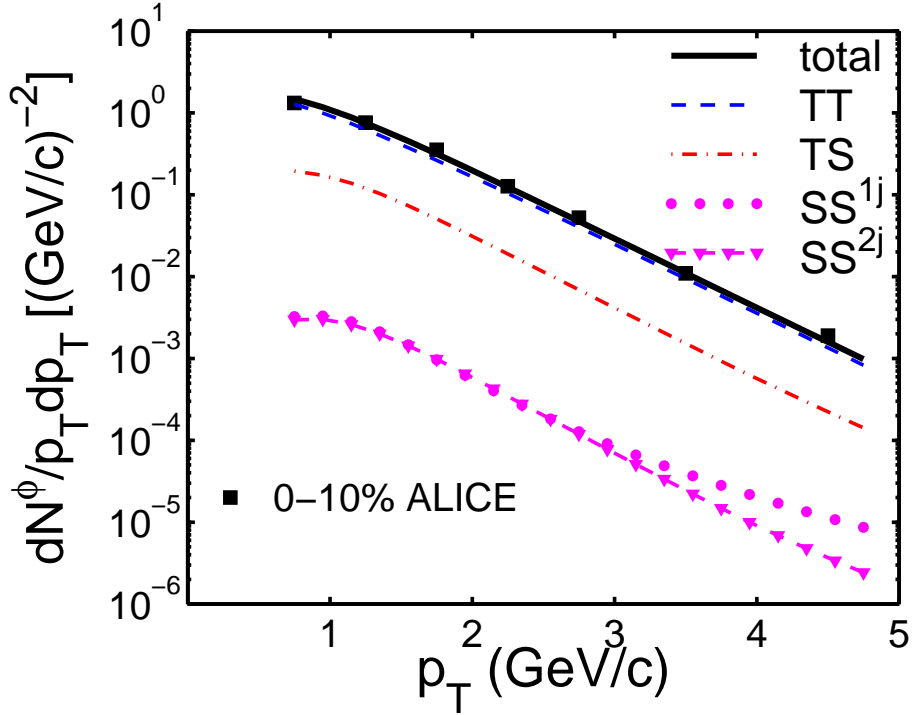


FIG. 16: (Color online) Transverse momentum distribution of  $\phi$  produced in Pb-Pb collision at  $\sqrt{s_{NN}} = 2.76$  TeV. Data are from [23] for centrality 0-10%.

The small value of  $g_\phi$  is an indication of quarkonium suppression after  $\phi$  is formed at a time much earlier than  $\pi$ , when the density of  $s$  (and  $\bar{s}$ ) is higher. As is the case with  $J/\psi$  suppression,  $\phi$  experiences the effects of dissociation by the plasma as it traverses the remaining portion of the medium before it completely hadronizes. The value of  $g_\phi$  depends on aspects of the process that are not included in the formalism discussed in this paper, and therefore cannot be predicted. The same remarks can be made for the formation of  $\Xi$  and  $\Omega$ , for which  $g_\Xi$  and  $g_\Omega$  are quite small in Eqs. (53) and (54).

### VIII. CONCLUSION

We have made a thorough study of the production of all identified hadrons in Pb-Pb collisions at LHC in a formalism that displays all the components of thermal- and shower-parton recombination. The degradation of momenta of hard and semihard partons is treated in a

way that uses two free parameters, which are determined by fitting the high- $p_T$  distribution of the pion. The resultant shower-parton distributions of  $q$  and  $s$  quarks are then used to calculate the spectra of all hadrons ( $\pi$ ,  $K$ ,  $p$ ,  $\Lambda$ ,  $\Xi$ ,  $\Omega$  and  $\phi$ ). They agree well with the data for all  $p_T$  up to 20 GeV/c. The description not only establishes a consistent scheme for treating the hadronization process of a quark-gluon plasma at LHC, but also points out the importance of the effects of minijets on the pion and proton distributions at low and intermediate  $p_T$  — yet not at all on the  $\phi$  and  $\Omega$  distributions on the other end of the spectrum in strangeness content.

The dominance of light shower partons over the thermal partons in nearly the whole range of parton momenta is an observation we make on the basis of an adopted form of the thermal parton distribution  $\mathcal{T}(p_1)$ . While the shower parton distribution  $\mathcal{S}(p_1)$  can be calculated, we have no dynamical scheme to calculate  $\mathcal{T}(p_1)$ , which is at the final stage of the evolution of the dense medium, dilute enough to enter into the confinement process. Since hadronization is insensitive to the initial process in which the dense medium is created, we have used the  $\mathcal{T}(p_1)$  determined at RHIC, where thermal partons dominate the low- $p_T$  region of all particles produced. The use of that  $\mathcal{T}(p_1)$  for our treatment at LHC is justified by the fact that ALICE data  $\pi$  and  $p$  distributions at low  $p_T$  are well reproduced by our results in which TS and TTS components dominate. Any more (or less) thermal partons would not have resulted in satisfactory fits of the low- $p_T$  data, since the density of soft shower partons is constrained by the fragmentation of hard and semihard jets. It is therefore meaningful to compare  $\mathcal{S}(p_1)$  with  $\mathcal{T}(p_1)$  and arrive at the conclusion that there are far more soft shower partons than thermal parton at LHC. It then follows that any theoretical treatment of hadrons produced at low  $p_T$  would be incomplete without taking the effects of minijets into account. In particular, the parameters in the hydrodynamical formalism cannot be determined by phenomenology in the soft sector without including also the soft partons from minijets.

It may be of interest to mention here that there is a phenomenological two-component model, in which the hard component exerts a strong influence on the production of pions in the low- $p_T$  region to the extent that the validity of hydrodynamical treatment of soft hadrons is questioned [50]. Although the physical basis for that observation may share some common ground with what we have found here (despite the very different languages and concepts used), it should be emphasized that our shower partons are dominant only at LHC, whereas

Ref. [50] contends the importance of the hard component in the soft region even at RHIC.

The dominance of  $\mathcal{S}(p_1)$  over  $\mathcal{T}(p_1)$  for production of  $\pi$  and  $p$  does not apply to  $\phi$  and  $\Omega$ . The  $s$  quarks in the shower are suppressed, so TS and TTS are lower than TT and TTT, respectively. The other particles ( $K, \Lambda$  and  $\Xi$ ) with less strangeness contents are in the intermediate situation. The recombination of thermal partons as the mechanism for the production of  $\phi$  and  $\Omega$  is therefore a satisfactory explanation for their  $p_T$  distributions up to 6.5 GeV/c that is too high for hydrodynamics and too abundantly produced for fragmentation.

A serious consequence of our conclusion about shower partons dominating over thermal partons is its implication on azimuthal anisotropy in non-central collisions. The usual explanation is that the azimuthal harmonics are due to the flow effects of the fluctuations of the initial configuration of the collision system. If, however, the non-flow effects such as minijets are important, the fluid treatment would be inadequate on the one hand, and our approach is in need of suitable treatment to be convincing on the other. For Au-Au collisions at 200 GeV, we have shown that the azimuthal harmonics can be obtained by taking into account the azimuthal dependence of minijet and the related ridge effect [17]. Now for Pb-Pb collisions at 2.76 TeV we have only investigated the case of central collisions here. To extend the study to non-central collisions is, of course, the natural problem to pursue next. How minijets influence the azimuthal asymmetry will undoubtedly be a major area of investigation. The consideration described here represents only the first, but significant, step toward understanding the physics of hadronization at LHC.

## Acknowledgment

This work was supported, in part, by the NSFC of China under Grant No. 11205106 and by the U. S. Department of Energy under Grant No. DE-FG02-96ER40972.

## Appendix A: Hadron Distribution at RHIC Revisited

Although the problem of hadron production at RHIC has been extensively studied previously [11, 14], we have made progressive improvement on the treatment of momentum degradation. In order to make sensible comparison between LHC and RHIC results, we

recalculated here the pion and proton distributions at RHIC, using the same description of the effects of energy loss on the shower partons, as has been done in Sec. IV.

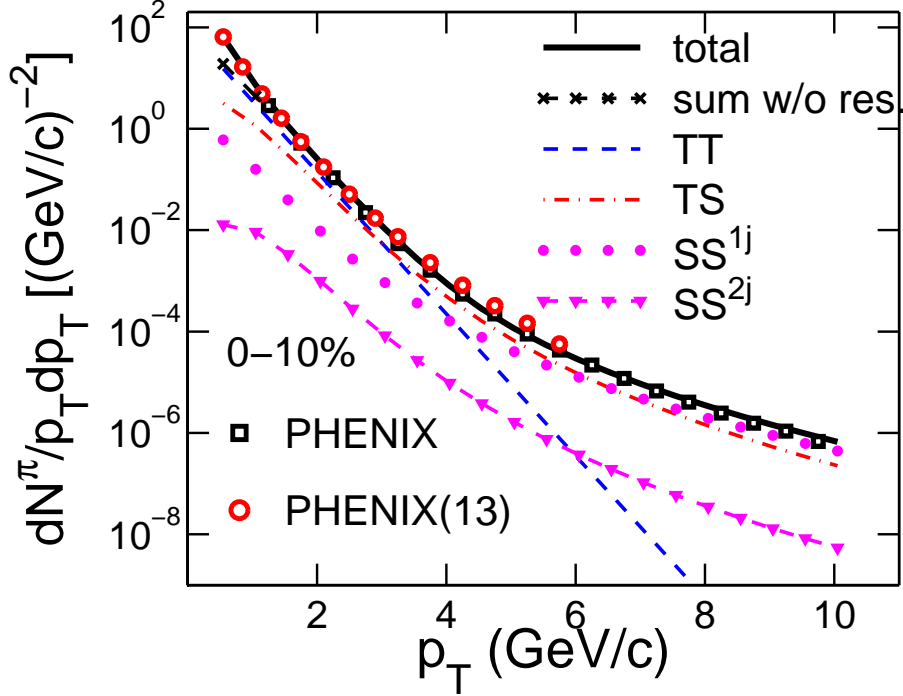


FIG. 17: (Color online) Transverse momentum distribution of pion produced in Au-Au collision at  $\sqrt{s_{NN}} = 200$  GeV. Data are from [20] for centrality 0-10%.

The basic difference between what we do now and what was done in Ref. [14] is that  $\gamma_g(q)$  is  $q$  dependent as given in Eq. (17). Keeping  $T = 0.31$  GeV as in Eq. (43), as well as in Ref. [11], we vary  $\gamma_0$  to find the best fit of the  $\pi$  distribution in Au-Au collisions at 200 GeV for 0-10% centrality, with  $q_0 = 10$  GeV/c fixed, as in Eq. (45). The initial parton distribution  $f_i(k)$  are as given in Ref. [34], and the recombination equation are the same as those in Sec. VI. With  $\gamma_0 = 0.6$ , we obtain the results shown in Fig. 17 for pion and Fig. 18 for proton, which are evidently very good. Comparing Fig. 17 to the pion distribution at LHC in Fig. 9, one can see the drastic difference in TS relative to TT between the two cases. At RHIC TS crosses TT at  $p_T \approx 3$  GeV/c, whereas at LHC it occurs at  $p_T \approx 0.5$  GeV/c. The latter is a consequence of  $\mathcal{S}(p_1) > \mathcal{T}(p_1)$  for  $p_1 > 0.5$  GeV/c, shown in Fig. 5. In contrast, at RHIC that cross-over does not occur until  $p_1 > 2$  GeV/c, as shown in Fig. 19. The ratio of  $\mathcal{S}/\mathcal{T}$  is already previewed in Fig. 6(a). Thus at RHIC  $\mathcal{S}(p_1)$  is a factor of 7 lower than that at LHC for  $p_1 < 2$  GeV/c. The low density of shower partons makes the

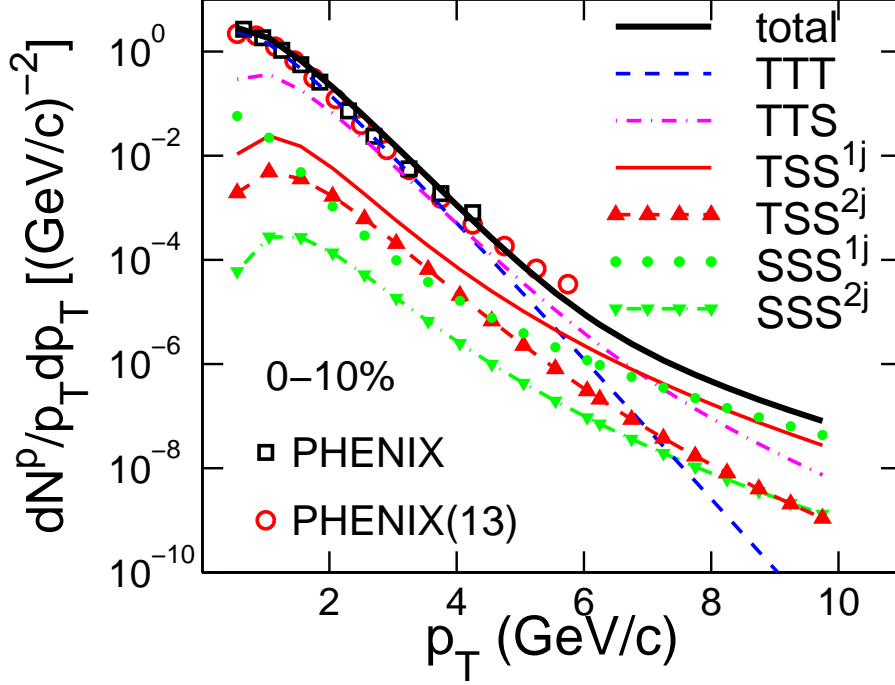


FIG. 18: (Color online) Transverse momentum distribution of proton produced in Au-Au collision at  $\sqrt{s_{NN}} = 200$  GeV. Data are from [20] for centrality 0-10%.

hydrodynamical treatment of thermal partons to be sensible without concern for minijets, which is not the case at LHC.

### Appendix B: Thermal Parton Distribution

The thermal parton distribution is given in Eq. (6) and the parameters  $C$  and  $T$  are given in Eq. (43). Section IV-A contains extensive discussion on why the thermal distribution  $\mathcal{T}(p_1)$  remains the same at LHC as it is at RHIC. In short, at late time when the bulk system is ready for hadronization its local properties at midrapidity are insensitive to its early history, except in very low  $p_1$  region ( $< 0.5$  GeV/c) where the enhanced thermal partons due to the energy lost by the semihard partons to the medium becoming even more enhanced at LHC. In this Appendix we show that different sets of higher values of  $C$  and  $T$  lead to  $p_T$  distributions of  $\pi$  and  $p$  that are unacceptable for  $p_T > 1$  GeV/c.

All equations we use to calculate the pion and proton spectra are as before, namely: Eq. (6) for  $\mathcal{T}(p_1)$ , (7) for  $\mathcal{S}(p_3)$ , (32)-(35) for  $dN_\pi/p_T dp_T$ , and (36)-(42) for  $dN_p/p_T dp_T$ .

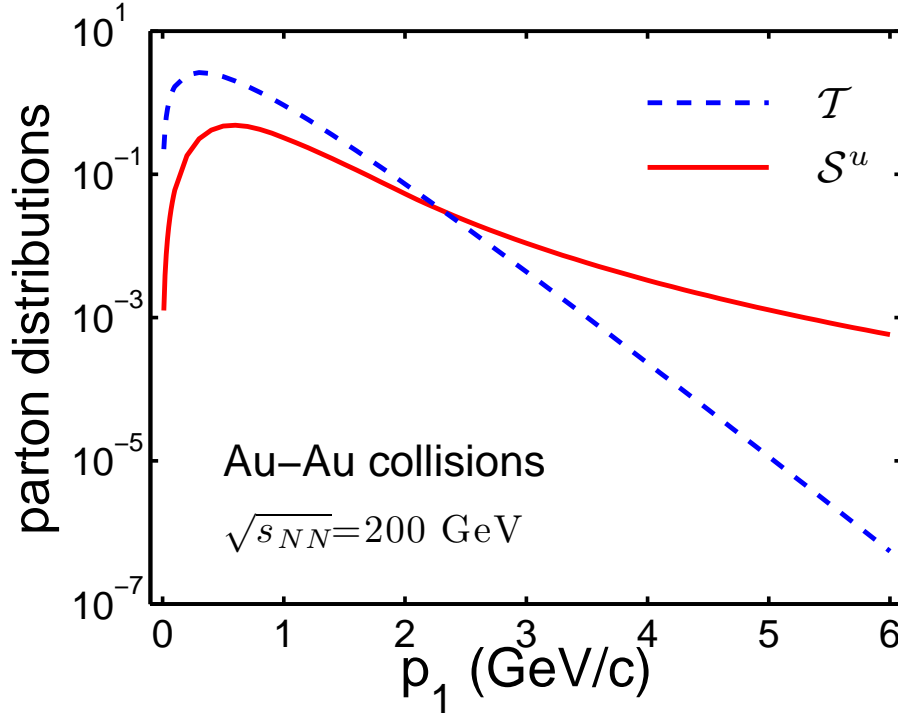


FIG. 19: (Color online) Thermal distribution  $\mathcal{T}(p_1)$  for Au-Au collisions at  $\sqrt{s_{NN}} = 200$  GeV is depicted by the dashed (blue) line for  $T = 0.31$  GeV, while the shower parton distribution  $\mathcal{S}^u$  is shown by the solid (red) line with low- $p_1$  cutoff.

The only changes are in the parameters  $C$  and  $T$ . For our demonstration here, we use the four combinations of  $C = 23.2$  and  $30$  GeV/c $^{-1}$ , and  $T = 0.31$  and  $0.4$  GeV/c. The results are shown in Figs. 20 and 21. The solid black lines are the ones corresponding to the universal values of  $C$  and  $T$  given in Eq. (43). The other three lines are for larger values of either  $C$ , or  $T$ , or both. Evidently, all of them far exceed the data in the  $p_T$  range shown and must be rejected. We have not exhibited the components  $TT, TS, \dots, TTT, TTS, \dots$  etc. for each case for the sake of clarity; however, it is obvious that the thermal-shower recombination raises the contribution at intermediate  $p_T$  significantly above the data when  $\mathcal{T}(p_1)$  is increased. We have not changed  $\mathcal{S}(p_2)$  so SS and SSS terms are not affected and remain the only dominant terms when  $p_T$  is high enough.

Our conclusion is therefore that with the shower parton distribution  $\mathcal{S}(p_2)$  fixed by the phenomenology at high  $p_T$ , only the thermal parton distribution described by  $C$  and  $T$  given in Eqs. (6) and (43) can reproduce the  $p_T$  spectra of  $\pi$  and  $p$  for  $p_T > 1$  GeV/c.



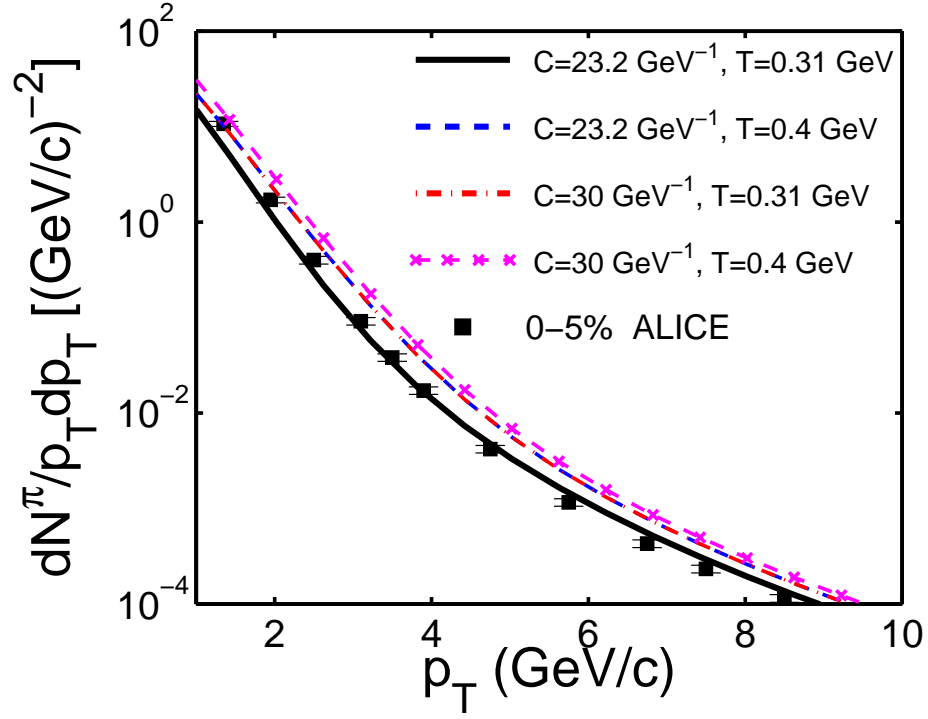


FIG. 20: (Color online) Pion distributions for four sets of values of  $C$  and  $T$ .

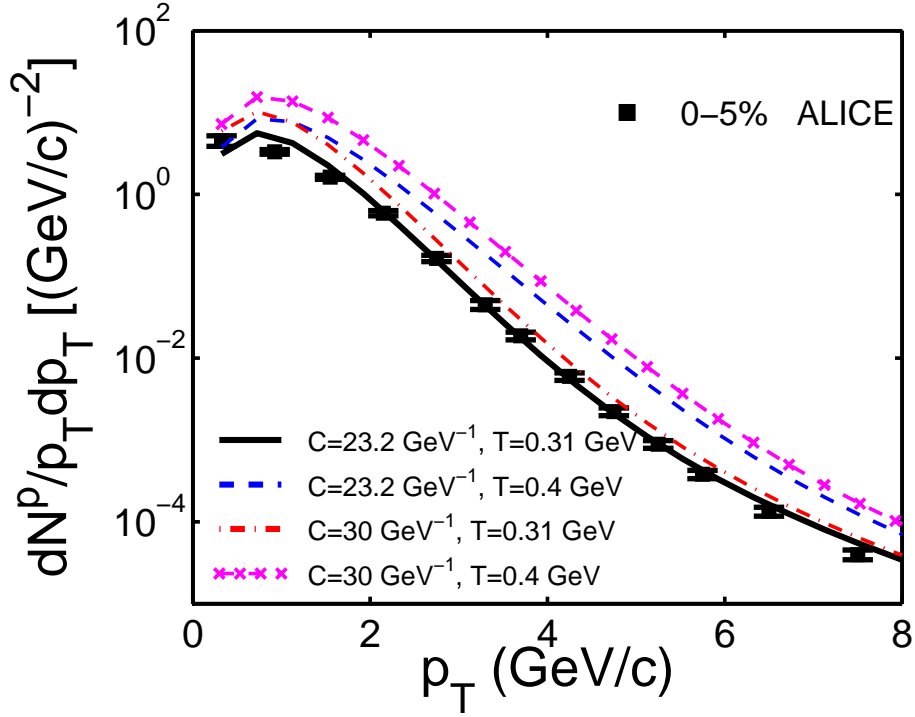


FIG. 21: (Color online) Proton distributions for four sets of values of  $C$  and  $T$ .

### Appendix C: $p_T$ Distribution of $\Lambda$ at LHC

The  $p_T$  distribution of  $\Lambda$  is very similar to that of proton except for the replacement of a  $u$  quark by an  $s$  quark. The thermal and shower parton distributions for  $s$  are different from those for  $u$ , and the RF for  $\Lambda$  is different from that for  $p$ . For  $\mathcal{T}^s(p_1)$  we use the same form as Eq. (46), but allow  $T_s$  to be adjustable.  $\mathcal{S}^s(p_2)$  is the same as used for  $K$  production in Sec. VI-B. The RF for  $\Lambda$  has the same form as Eq. (9) for proton but with  $\alpha = 1$  and  $\beta = 2$  in a problem on strange particle production at RHIC considered in Ref. [45]. We simply list the equation below for the various components.

$$\frac{dN_{\Lambda}^{TTT}}{p_T dp_T} = \frac{g_{st}^{\Lambda} g_{\Lambda} C^3}{m_T^p p_T^{2\alpha+\beta+3}} \int_0^{p_T} dp_1 \int_0^{p_T-p_1} dp_2 \times (p_1 p_2)^{\alpha+1} e^{-(p_1+p_2)/T} (p_T - p_1 - p_2)^{\beta+1} e^{-(p_T-p_1-p_2)/T_s}, \quad (C1)$$

$$\begin{aligned} \frac{dN_{\Lambda}^{TTS}}{p_T dp_T} = & \frac{g_{st}^{\Lambda} g_{\Lambda} C^2}{m_T^p p_T^{2\alpha+\beta+3}} \int_0^{p_T} dp_1 \int_0^{p_T-p_1} dp_2 \\ & \times \left\{ p_1 p_2 e^{-(p_1+p_2)/T} (p_1 p_2)^{\alpha} (p_T - p_1 - p_2)^{\beta} \mathcal{S}^s(p_T - p_1 - p_2) \right. \\ & \left. + p_1 e^{-p_1/T} p_2 e^{p_2/T_s} p_1^{\alpha} p_2^{\beta} (p_T - p_1 - p_2)^{\alpha} \mathcal{S}^u(p_T - p_1 - p_2) \right\}, \quad (C2) \end{aligned}$$

$$\begin{aligned} \frac{dN_{\Lambda}^{TSS^{1j}}}{p_T dp_T} = & \frac{g_{st}^{\Lambda} g_{\Lambda} C}{m_T^{\Lambda} p_T^{2\alpha+\beta+3}} \int_0^{p_T} dp_1 \int_0^{p_T-p_1} dp_2 \\ & \times \left\{ p_1 e^{-p_1/T_s} p_1^{\beta} p_2^{\alpha} (p_T - p_1 - p_2)^{\alpha} \mathcal{S}^{ud}(p_2, p_T - p_1 - p_2) \right. \\ & \left. + p_1 e^{-p_1/T} (p_1 p_2)^{\alpha} (p_T - p_1 - p_2)^{\beta} \mathcal{S}^{ds}(p_2, p_T - p_1 - p_2) \right\}, \quad (C3) \end{aligned}$$

$$\begin{aligned} \frac{dN_{\Lambda}^{TSS^{2j}}}{p_T dp_T} = & \frac{g_{st}^{\Lambda} g_{\Lambda} C \Gamma}{m_T^{\Lambda} p_T^{2\alpha+\beta+3}} \int_0^{p_T} dp_1 \int_0^{p_T-p_1} dp_2 \\ & \times \left\{ p_1 e^{-p_1/T_s} p_1^{\beta} p_2^{\alpha} (p_T - p_1 - p_2)^{\alpha} \mathcal{S}^u(p_2) \mathcal{S}^d(p_T - p_1 - p_2) \right. \\ & \left. + p_1 e^{-p_1/T} (p_1 p_2)^{\alpha} (p_T - p_1 - p_2)^{\beta} \mathcal{S}^d(p_2) \mathcal{S}^s(p_T - p_1 - p_2) \right\}, \quad (C4) \end{aligned}$$

$$\frac{dN_{\Lambda}^{SSS^{1j}}}{p_T dp_T} = \frac{1}{m_{\Lambda}^T} \int \frac{dq}{q^2} \sum_i \hat{F}_i(q) D_i^{\Lambda}(p_T, q), \quad (C5)$$

$$\begin{aligned} \frac{dN_{\Lambda}^{SSS^{2j}}}{p_T dp_T} &= \frac{g_{st}^{\Lambda} g_{\Lambda} \Gamma}{m_T^{\Lambda} p_T^{2\alpha+\beta+3}} \int_0^{p_T} dp_1 \int_0^{p_T-p_1} dp_2 \\ &\times \left\{ p_1^{\beta} p_2^{\alpha} (p_T - p_1 - p_2)^{\alpha} \mathcal{S}^s(p_1) \mathcal{S}^{ud}(p_2, p_T - p_1 - p_2) \right. \\ &\left. + (p_1 p_2)^{\alpha} (p_T - p_1 - p_2)^{\beta} \mathcal{S}^u(p_1) \mathcal{S}^{ds}(p_2, p_T - p_1 - p_2) \right\}, \quad (\text{C6}) \end{aligned}$$

The statistical factor is  $g_{st}^{\Lambda} = 1/8$ , and the prefactor from RF is  $g_{\Lambda} = [B(\alpha + 1, \alpha + \beta + 2)B(\alpha + 1, \beta + 1)]^{-1}$ . The corresponding FFs,  $D_i^{\Lambda}(z)$ , are given by AKK [46] by fitting the data at next-leading-order (NLO).

#### Appendix D: $p_T$ Distribution of $\Xi$ at LHC

For the recombination of  $dss$  to form  $\Xi$  we make the simplifying assumption that the RF is proportional to  $\delta$ -functions, i.e.,  $\prod_{i=1}^3 \delta(p_i - p_T/3)$ . Then it is straightforward to write the distributions

$$\frac{dN_{\Xi}^{TTT}}{p_T dp_T} = \frac{g_{\Xi} C^3 p_T^2}{27 m_T^{\Xi}} e^{-p_T/3T} e^{-2p_T/3T_s}, \quad (\text{D1})$$

$$\frac{dN_{\Xi}^{TTS}}{p_T dp_T} = \frac{g_{\Xi} C^2 p_T}{9 m_T^{\Xi}} \left\{ e^{-\frac{p_T}{3}(\frac{1}{T} + \frac{1}{T_s})} \mathcal{S}^s(p_T/3) + e^{-\frac{2p_T}{3T_s}} \mathcal{S}^u(p_T/3) \right\}, \quad (\text{D2})$$

$$\frac{dN_{\Xi}^{TSS^{1j}}}{p_T dp_T} = \frac{g_{\Xi} C}{3 m_T^{\Xi}} \left\{ e^{-\frac{p_T}{3T}} \mathcal{S}^{ss}(p_T/3, p_T/3) + e^{-\frac{p_T}{3T_s}} \mathcal{S}^{us}(p_T/3, p_T/3) \right\}, \quad (\text{D3})$$

$$\frac{dN_{\Xi}^{TSS^{2j}}}{p_T dp_T} = \frac{g_{\Xi} C \Gamma}{3 m_T^{\Xi}} \left\{ e^{-\frac{p_T}{3T}} \mathcal{S}^s(p_T/3, ) \mathcal{S}^s(p_T/3) + e^{-\frac{p_T}{3T_s}} \mathcal{S}^u(p_T/3) \mathcal{S}^s(p_T/3) \right\}, \quad (\text{D4})$$

$$\frac{dN_{\Xi}^{SSS^{1j}}}{p_T dp_T} = \frac{g_{\Xi}}{p_T m_T^{\Xi}} \mathcal{S}^{uss}(p_T/3, p_T/3, p_T/3), \quad (\text{D5})$$

$$\frac{dN_{\Xi}^{SSS^{2j}}}{p_T dp_T} = \frac{g_{\Xi} \Gamma}{p_T m_T^{\Xi}} \left\{ \mathcal{S}^u(p_T/3) \mathcal{S}^{ss}(p_T/3, p_T/3) + \mathcal{S}^s(p_T/3) \mathcal{S}^{us}(p_T/3, p_T/3) \right\}, \quad (\text{D6})$$

where

$$\mathcal{S}^{dss}(p_1, p_2, p_3) = \int \frac{dq}{q} \sum_i \hat{F}_i(q) S_i^u(p_1, q) S_i^s(p_2, q - p_1) S_i^s(p_3, q - p_1 - p_2). \quad (\text{D7})$$

### Appendix E: $p_T$ Distribution of $\Omega$ at LHC

With the RF for  $\Omega$  assumed to be  $\prod_{i=1}^3 \delta(p_i - p_T/3)$ , as it is for  $\Xi$ , the distributions for the different components are simplest of all baryons, since all constituent quarks are the same.

We have

$$\frac{dN_{\Omega}^{TTT}}{p_T dp_T} = \frac{g_{\Omega} C^3 p_T^2}{27 m_T^{\Omega}} e^{-p_T/T_s}, \quad (\text{E1})$$

$$\frac{dN_{\Omega}^{TTS}}{p_T dp_T} = \frac{g_{\Omega} C^2 p_T}{9 m_T^{\Omega}} e^{-2p_T/3T_s} \mathcal{S}^s(p_T/3), \quad (\text{E2})$$

$$\frac{dN_{\Omega}^{TSS^{1j}}}{p_T dp_T} = \frac{g_{\Omega} C}{3 m_T^{\Omega}} e^{-p_T/3T_s} \mathcal{S}^{ss}(p_T/3, p_T/3), \quad (\text{E3})$$

$$\frac{dN_{\Omega}^{TSS^{2j}}}{p_T dp_T} = \frac{g_{\Omega} C \Gamma}{3 m_T^{\Omega}} e^{-p_T/3T_s} \mathcal{S}^s(p_T/3) \mathcal{S}^s(p_T/3), \quad (\text{E4})$$

$$\frac{dN_{\Omega}^{SSS^{1j}}}{p_T dp_T} = \frac{g_{\Omega}}{p_T m_T^{\Omega}} \mathcal{S}^{sss}(p_T/3, p_T/3, p_T/3), \quad (\text{E5})$$

$$\frac{dN_{\Omega}^{SSS^{2j}}}{p_T dp_T} = \frac{g_{\Omega} \Gamma}{p_T m_T^{\Omega}} \mathcal{S}^s(p_T/3) \mathcal{S}^{ss}(p_T/3, p_T/3). \quad (\text{E6})$$

Apart from the prefactor that involves  $p_T^2/m_T^{\Omega}$ , the TTT term is a pure exponential. If it is dominant, then the  $p_T$  dependence of Eq. (E1) is a direct test of the validity of our description of  $\Omega$  production.

### Appendix F: $p_T$ Distribution of $\phi$ at LHC

As it is for  $\Omega$ , the distributions for  $\phi$  is simple when the RF is taken to be  $\prod_{i=1}^2 \delta(p_i - p_T/2)$  for  $s\bar{s}$  recombination. One gets

$$\frac{dN_{\phi}^{TT}}{p_T dp_T} = \frac{g_{\phi} C^2 p_T}{4 m_T^{\phi}} e^{-p_T/T_s}, \quad (\text{F1})$$

$$\frac{dN_\phi^{TS}}{p_T dp_T} = \frac{g_\phi C}{2m_T^\phi} e^{-p_T/2T_s} \mathcal{S}^s(p_T/2), \quad (\text{F2})$$

$$\frac{dN_\phi^{SS^{1j}}}{p_T dp_T} = \frac{g_\phi}{p_T m_T^\phi} \mathcal{S}^{s\bar{s}}(p_T/2, p_T/2), \quad (\text{F3})$$

$$\frac{dN_\phi^{SS^{2j}}}{p_T dp_T} = \frac{g_\phi \Gamma}{p_T m_T^\phi} \mathcal{S}^s(p_T/2) \mathcal{S}^{\bar{s}}(p_T/2). \quad (\text{F4})$$

- 
- [1] P. Braun-Munzinger, K. Redlich and J. Stachel, in *Quark-Gluon Plasma 3*, edited by R. C. Hwa and X.-N. Wang (World Scientific, Singapore, 2004), p. 491.
  - [2] P. Huovinen, in *Quark-Gluon Plasma 3*, edited by R. C. Hwa and X.-N. Wang (World Scientific, Singapore, 2004), p. 600.
  - [3] P. F. Kolb and U. Heinz, in *Quark-Gluon Plasma 3*, edited by R. C. Hwa and X.-N. Wang (World Scientific, Singapore, 2004), p. 634.
  - [4] D. A. Teaney, in *Quark-Gluon Plasma 4*, edited by R. C. Hwa and X.-N. Wang (World Scientific, Singapore, 2010), p. 207.
  - [5] C. Gale, S. Jeon, and B. Schenke, Int. J. Mod. Phys. A **28**, 1340010 (2013).
  - [6] R. Baier, Y. L. Dokshitzer, A. H. Mueller, S. Peigne and D. Schiff, Nucl. Phys. B **483**, 291 (1997); **484**, 265 (1997).
  - [7] X.-F. Guo and X.-N. Wang, Phys. Rev. Lett. **85**, 3591 (2000); X.-N. Wang and X.-F. Guo, Nucl. Phys. A **696**, 788 (2001).
  - [8] A. Majumder and M. Van Leeuwen, Prog. Part. Nucl. Phys. A **66**, 41(2011).
  - [9] Y. Mehtar-Tami, J. G. Milhano and K. Tywoniuk, Int. J. Mod. Phys. A **28**, 1340013 (2013).
  - [10] K. M. Burke *et al.* (JET Collaboration) arXiv: 1312.5003.
  - [11] R. C. Hwa and C. B. Yang, Phys. Rev. C **70**, 024905 (2004).
  - [12] R. C. Hwa and C. B. Yang, Phys. Rev. C **75**, 054904 (2007).
  - [13] R. C. Hwa and Lilin Zhu, Phys. Rev. C **84**, 064914 (2011).

- [14] Lilin Zhu and R. C. Hwa, Phys. Rev. C **88**, 044919 (2013).
- [15] R. C. Hwa, Phys. Lett. B **666**, 228 (2008).
- [16] C. B. Chiu, R. C. Hwa and C. B. Yang, Phys. Rev. C **78**, 044903 (2008).
- [17] R. C. Hwa and L. Zhu, Phys. Rev. C **86**, 024901 (2012).
- [18] P. Steinberg, (ATLAS collaboration) J. Phys. G **38**, 124004(2011).
- [19] K. Aamodt *et al.* (ALICE collaboration), Phys. Rev. Lett. **105**, 252301(2010).
- [20] A. Adare *et al.* (PHENIX Collaboration), Phys. Rev. Lett. **101**, 232301 (2008); Phys. Rev. C **87**, 034911 (2013); Phys. Rev. C **88**, 024906(2013). S. S. Adler, *et al* (PHENIX Collaboration), Phys. Rev. Lett **91**, 072301(2003); Phys. Rev. C **69**, 034909(2004).
- [21] Xianglei Zhu, (STAR collaboration), talk given at Quark Matter 2014. The preliminary data for  $\Omega$  production in Au-Au collisions.
- [22] M. Ivanov, (ALICE collaboration), Nucl. Phys. A **904**, 162c(2013).
- [23] B. Abelev *et al.* (ALICE Collaboration), Phys. Lett. B **728**, 216(2014).
- [24] B. A. Kniehl, G. Kramer and B. Pötter, Nucl. Phys. B **597**, 337(2001).
- [25] R. C. Hwa and C. B. Yang, Phys. Rev. C **67**, 034902 (2003).
- [26] R. C. Hwa and C. B. Yang, Phys. Rev. C **81**, 024908 (2010).
- [27] R. C. Hwa and C. B. Yang, Phys. Rev. C **70**, 024904 (2004).
- [28] R. C. Hwa and C. B. Yang, Phys. Rev. C **73**, 064904 (2006).
- [29] K. P. Das AND R. C. Hwa, Phys. Lett. B **68**, 459 (1977).
- [30] R. C. Hwa, Phys. Rev. D **22**, 1593 (1980).
- [31] R. C. Hwa and C. B. Yang, Phys. Rev. C **65**, 034905 (2002).
- [32] R. C. Hwa and C. B. Yang, Phys. Rev. C **66**, 025204 (2002).
- [33] S. S. Adler *et al.* (PHENIX Collaboration), Phys. Rev. C **69**, 034909 (2004).
- [34] D. K. Srivastava, C. Gale, and R. J. Fries, Phys. Rev. C **67**, 034903 (2003).
- [35] S. S. Adler *et al.* (PHENIX Collaboration), Phys. Rev. C **69**, 034909 (2004).
- [36] S. S. Adler *et al.* (PHENIX Collaboration), Phys. Rev. Lett. **91**, 072301 (2003).
- [37] A. Adare *et al.* (PHENIX Collaboration), Phys. Rev. Lett. **101**, 232301 (2008); Phys. Rev. C **87**, 034911 (2013).
- [38] B. I. Abelev *et al.*, (STAR Collaboration), Phys. Rev. Lett. **97**, 152301 (2006).
- [39] A. Agakishiev *et al.*, (STAR Collaboration), Phys. Rev. Lett. **108**, 072302 (2012).
- [40] A. Adare *et al.* (PHENIX Collaboration), arXiv: 1304.3410 (2013).

- [41] B. Abelev *et al.*, (ALICE Collaboration), Phys. Lett. B. **720**, 52 (2013).
- [42] C. Tsallis, Stat. Phys. **52**, 479 (1988).
- [43] K. Aamodt *et al.*, (ALICE Collaboration), Phys. Lett. Lett. **106**, 032301 (2011).
- [44] R. C. Hwa and C. B. Yang, Phys. Rev. C **66**, 025205 (2002).
- [45] R. C. Hwa and C. B. Yang, Phys. Rev. C **75**, 054904 (2007).
- [46] S. Albino, B. A. Kniehl and G. Kramer, J. Phys. G: Nucl. Part. Phys. **34**, S789 (2007).
- [47] B. Abelev *et al.* (ALICE Collaboration), Phys. Lett. Lett. **111**, 222301 (2013).
- [48] J. Adams *et al.* (STAR Collaboration), Phys. Lett. Lett. **92**, 182301 (2004).
- [49] R. C. Hwa, J. Phys. G: Nucl. Part. Phys. **34**, S789 (2007).
- [50] T. A. Trainor, Int. J. Mod. Phys. E **17**, 1499 (2008); Phys. Rev. C **80**, 044901 (2009).